Title

ADRAM is an experience-dependent long noncoding RNA that drives fear extinction through a direct interaction with the chaperone protein 14-3-3

Journal

Cell Reports, 38(12)

ISSN

2639-1856

Authors

Wei, Wei
Zhao, Qiongyi
Wang, Ziqi
et al.

Publication Date

2022-03-01

DOI

10.1016/j.celrep.2022.110546

HHS Public Access

Author manuscript

Cell Rep. Author manuscript; available in PMC 2022 April 18.

Published in final edited form as:

Cell Rep. 2022 March 22; 38(12): 110546. doi:10.1016/j.celrep.2022.110546.

ADRAM is an experience-dependent long noncoding RNA that drives fear extinction through a direct interaction with the chaperone protein 14-3-3

Wei Wei[1,2,7,8,*], **Qiongyi Zhao**[3,8], **Ziqi Wang**[3], **Wei-Siang Liau**[3], **Dean Basic**[3], **Haobin Ren**[3], **Paul R. Marshall**[3], **Esmi L. Zajaczkowski**[3], **Laura J. Leighton**[3], **Sachithrani U. Madugalle**[3], **Mason Musgrove**[3], **Ambika Periyakaruppiah**[3], **Jichun Shi**[1,2], **Jianjian Zhang**[1], **John S. Mattick**[4], **Timothy R. Mercer**[5], **Robert C. Spitale**[6], **Xiang Li**[1,2,7], **Timothy W. Bredy**[3,9,*]

[1]Department of Neurosurgery, Zhongnan Hospital of Wuhan University, Wuhan, China

[2]Brain Research Center, Zhongnan Hospital of Wuhan University, Wuhan, China

[3]Cognitive Neuroepigenetics Laboratory, Queensland Brain Institute, The University of Queensland, Brisbane, Australia

[4]School of Biotechnology and Biomolecular Sciences, The University of New South Wales, Sydney, Australia

[5]Australian Institute of Bioengineering and Nanotechnology, The University of Queensland, Brisbane, Australia

[6]Department of Pharmaceutical Sciences, University of California, Irvine, Irvine, USA

[7]Medical Research Institute, Wuhan University, Wuhan, China

[8]These authors contributed equally

[9]Lead contact

SUMMARY

Here, we used RNA capture-seq to identify a large population of lncRNAs that are expressed in the infralimbic prefrontal cortex of adult male mice in response to fear-related learning. Combining these data with cell-type-specific ATAC-seq on neurons that had been selectively activated by fear extinction learning, we find inducible 434 lncRNAs that are derived from enhancer regions in the vicinity of protein-coding genes. In particular, we discover an experience-induced lncRNA we call ADRAM (activity-dependent lncRNA associated with memory) that

*Correspondence: wei.wei@whu.edu.cn (W.W.), t.bredy@uq.edu.au (T.W.B.).

AUTHOR CONTRIBUTIONS

Conceptualization, T.W.B., W.W., and X.L.; experiments, X.L., Z.W., W.-S.L., P.R.M., J.S., E.L.Z., L.J.L., S.U.M., A.P., H.R., J.S., and J.Z.; computational analyses, D.B. and Q.Z.; data interpretation, T.W.B., W.W., Q.Z., and X.L.; writing – original draft, T.W.B., X.L., and W.W.; writing – review & editing, T.W.B., W.W., Q.Z., T.W.M., J.S.M., R.C.S., and X.L.

SUPPLEMENTAL INFORMATION

Supplemental information can be found online at https://doi.org/10.1016/j.celrep.2022.110546.

DECLARATION OF INTERESTS

The authors declare no competing interests.

acts as both a scaffold and a combinatorial guide to recruit the brain-enriched chaperone protein 14-3-3 to the promoter of the memory-associated immediate-early gene Nr4a2 and is required fear extinction memory. This study expands the lexicon of experience-dependent lncRNA activity in the brain and highlights enhancer-derived RNAs (eRNAs) as key players in the epigenomic regulation of gene expression associated with the formation of fear extinction memory.

Graphical Abstract

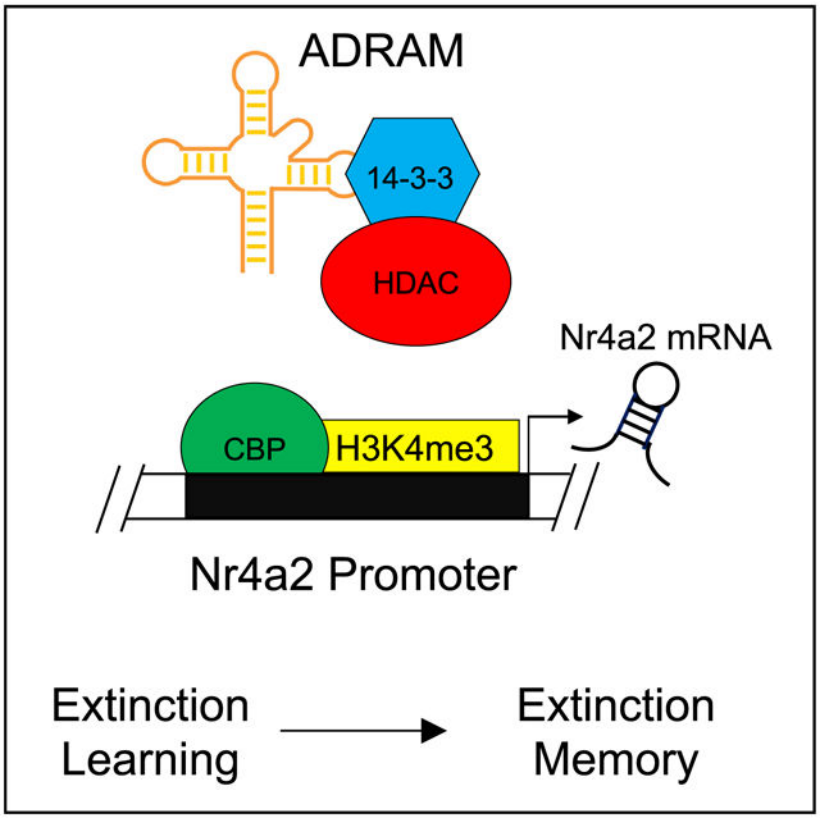

In brief

Wei et al. use targeted RNA capture sequencing to examine experience-dependent long noncoding RNA activity in the infralimbic prefrontal cortex of adult mice. They discover a gene, which they call ADRAM, that is directly involved in the epigenomic regulation of gene expression underlying memory formation.

INTRODUCTION

The extinction of conditioned fear, the reduction in responding to a feared cue, which occurs when the cue is repeatedly presented without any adverse consequence, is an evolutionarily conserved behavioral adaptation that is critical for survival. Like other forms of learning, long-lasting memory for fear extinction depends on coordinated changes in gene expression, particularly in the infralimbic prefrontal cortex (ILPFC) (Martin et al., 2000; Bruel-Jungerman et al., 2007; Alberini, 2009). In recent years, we and others have shown that

this process involves a tightly controlled interplay between the transcriptional machinery and epigenomic mechanisms (reviewed in Marshall and Bredy, 2019). Epigenetics in this context refers to the regulatory mechanisms that drive long-lasting effects in gene expression without a change to the underlying genetic code. Indeed, a wide variety of chromatin and DNA modifications have been shown to play an essential role in various forms of learning and the establishment of long-term memory (Bredy et al., 2007; Vecsey et al., 2007; Wei et al., 2012; Graff et al., 2014; Li et al., 2014, 2019; Feng et al., 2015; Lepack et al., 2020).

Although considerable progress has been made in understanding how epigenomic modifiers are directed to their requisite sites of action across the genome during early development, it remains to be fully determined how this specificity is conferred in the adult brain, particularly within the context of learning and memory. Long noncoding RNAs (lncRNAs) comprise a class of genes that have recently gained attention as important regulators of cellular function due to their multidimensional capacity to function as decoys for transcription factors, as guides to direct chromatin modifiers, or as modular scaffolds in the nucleus (Mercer and Mattick, 2013). LncRNAs, defined as any RNA longer than 200 nt and without protein-coding potential, are expressed in a highly cell-type and spatiotemporally specific manner in the adult brain (Mercer et al., 2008), with 40% of all lncRNAs identified to date shown to be enriched in neurons. It has therefore been proposed that lncRNAs are uniquely positioned to mediate rapid responses to environmental stimuli and to promote cognition (Spadaro and Bredy, 2012; Liau et al., 2021). In agreement with this idea, the nuclear-enriched lncRNA *Gm12371* influences hippocampal dendritic morphology and synaptic plasticity (Raveendra et al., 2018), the nuclear antisense lncRNA *AtLAS* regulates synapsin II polyadenylation and AMPA receptor trafficking (Ma et al., 2020), and an association between the lncRNA *LONA* and synaptic plasticity and spatial memory (Li et al., 2018) has been reported. Not surprisingly, lncRNAs have also been implicated in the regulation of gene expression underlying neuropsychiatric disorders characterized by impaired cognition, including drug addiction, depression, impulsivity, schizophrenia, and anxiety (Barry et al., 2014; Spadaro et al., 2015; Xu et al., 2020; Issler et al., 2020; Labonte et al., 2021).

Given the increasing recognition that lncRNAs play important roles in brain function, we considered their impact on fear extinction. We first used targeted RNA sequencing to reveal lncRNAs that were induced in response to fear-related learning and its extinction. The complex isoform architecture of the newly identified lncRNAs was then resolved by ATAC sequencing, with chromatin and RNA immunoprecipitation analysis being used to functionally characterize the lncRNA-mediated epigenomic regulation of target gene expression. Finally, lentiviral-mediated knockdown and antisense oligonucleotide (ASO) injections were used to investigate the causal mechanisms by which an enhancer-derived lncRNA BB557941, which we call ADRAM (activity-dependent lncRNA associated with memory), regulates the expression of the immediate-early gene Nr4a2 and drives the formation of fear extinction memory.

RESULTS

A substantial number of lncRNAs are expressed in the ILPFC in response to fear-related learning

Most lncRNAs are expressed in low abundance and with cell-type specificity. As a result, they are often missed during the analysis of complex tissues, such as the brain (Deveson et al., 2017). We therefore adopted a method called RNA capture sequencing (capture-seq), which provides the additional sensitivity required to determine the full repertoire of learning-induced lncRNAs in the adult ILPFC. RNA capture-seq uses tiling oligonucleotides to enrich for RNA targets of interest prior to sequencing, resulting in a dramatic increase in the sensitivity to detect rare transcripts (Mercer et al., 2011, 2014). In the following experiment, a panel targeting 190,689 probes comprising 28,228 known and predicted mouse lncRNAs, which was previously developed to improve the annotation of brain-enriched lncRNA (Bussotti et al., 2016), was used to identify lncRNAs in the ILPFC that are expressed in response to fear learning and during the formation of fear extinction memory. We trained mice using a standard cued fear-conditioning task followed by either novel context exposure (retention control [RC]) or extinction training (EXT) and, immediately after training, the ILPFC was extracted and RNA prepared for downstream analysis (Figure 1A).

Using RNA capture-seq, with an average of 68 million (83%) uniquely mapped reads per pooled library (Table S1), we identified a total of 23,514 lncRNAs that were expressed following RC or EXT, with many being novel (66%, 15,439) or listed in the GENCODE database as transcripts (14.5%, 3,412) of unknown function. *Meg3* (Chanda et al., 2018), *Malat1* (Wu and Yi, 2018), and *Gomafu* (Spadaro et al., 2015) were among the most abundantly expressed brain-enriched lncRNAs that have been functionally characterized, although no differential expression between RC and EXT mice was detected (Table S1). A transcript-level expression analysis comparing the RC and EXT groups revealed that none of the detected lncRNAs reached the threshold (FDR < 0.05) to be considered differentially expressed following learning. This is perhaps surprising given the historical reliance on concluding that a gene is relevant or causal based on whether it is up- or downregulated. However, emerging evidence indicates that the apparently low levels of expression of lncRNAs generally reflects their high cell-type specificity (Mercer et al., 2008; Cabili et al., 2015; Seiler et al., 2017; Deveson et al., 2017) and there are increasing examples of lncRNAs with highly restricted spatial expression that impact brain development and function (Cajigas et al., 2018; Hollensen et al., 2020; Perry et al., 2018; Raveendra et al., 2018; Wang et al., 2021; Grinman et al., 2021).

LncRNAs exhibit extreme variations in length, have a modular architecture, and undergo complex patterns of alternative splicing (Deveson et al., 2018), all of which can impact their functional activity independent of their level of expression. It is well established that lncRNAs exert their regulatory influence in a context- and state-dependent manner that is contingent on the cellular compartment in which they are expressed. In support of this idea, we previously observed this to be the case with the lncRNA *Gomafu* (*Miat*), which was found to function both in *cis* as a scaffold for the polycomb complex within the

local genome environment (Spadaro et al., 2015), and in *trans* as a decoy for the splicing factors QK1 and SRSF1 in the nucleolus (Barry et al., 2014). Moreover, although *Malat1* is one of the most highly abundant lncRNAs to be identified to date, its structural state is heavily influenced by RNA modification, which alters its ability to interact with specific RNA-binding proteins, thereby determining its functional state independent of transcript abundance (Liu et al., 2017). In addition, the lncRNA *Neat1* has a highly complex modular structure, which confers its ability to act as a scaffold in the assembly of paraspeckles through phase separation (Yamazaki et al., 2018). This may influence how it participates in behavioral responses to stress (Kukharsky et al., 2020) and as an architect of chromatin modification supporting age-related spatial memory processes (Butler et al., 2019). It is increasingly becoming evident that there are many factors beyond transcriptional abundance that determine whether an lncRNA is functionally relevant (Liau et al., 2021). Therefore, we decided to look more deeply into how lncRNAs are regulated in the ILPFC, and how they are functionally activated in response to fear extinction learning.

LncRNAs exhibit unique, context-dependent, chromatin accessibility profiles

LncRNAs are frequently found antisense, bidirectional, or in close proximity to key protein-coding genes. Furthermore, many lncRNAs mediate their actions in *cis* by regulating the local chromatin context of neighboring protein-coding genes. Based on this, we next analyzed the genomic organization of lncRNAs in cells that have been activated by learning. In an independent cohort of mice, the activity-regulated cytoskeleton-associated protein (*Arc*) and the neuronal nuclear marker *NeuN* were used to tag specific populations of neurons that had been selectively activated by RC or EXT, which were then isolated by fluorescence-activated cell sorting and prepared for downstream analysis (Li et al., 2019) (Figure S1). ATAC-seq (assay for transposase-accessible chromatin using sequencing) was applied to Arc+ neuronal populations in order to resolve the genome-wide landscape of chromatin accessibility following RC and EXT learning in activated neurons derived from the ILPFC. Overall, with an average of 86 million (86%) uniquely mapped reads per pooled library, we found that chromatin-accessible regions exhibited a similar genomic distribution in both conditions (Table S1; Figure S2).

Focusing on the Arc+ neurons of EXT mice, we found that accessible chromatin regions were more likely to be enriched at the 5′ untranslated region (UTR) (17.5%) rather than the 3′ UTR (2.5%), which occurred with a similar frequency to transcription start sites (TSSs) (16.8%) (Figure 1B). A significant proportion of ATAC peaks were found in intronic (43%) and intergenic (27.3%) regions, indicating a potentially rich source of active genomic regions from which many lncRNAs may be derived (Figure 1B). Indeed, the majority of expressed lncRNAs were found in either intragenic (11,496; 49% of total) or intergenic regions distal (>10 kb) to protein-coding genes (9,909; 42% of total). In addition, we found that 2,109 lncRNAs (~9% of total) were expressed in genomic regions in the vicinity (<10 kb) of protein-coding genes. Among these 2,109 proximal lncRNAs, 42% (892) were associated with open chromatin, which was markedly higher than the proportion of intergenic (16%) or intragenic (26%) lncRNAs (Table S1). A permutation test to determine whether the different regions are more likely to overlap than similar sized genomic regions

sampled by chance revealed that the highest overlap number from 1,000 permutation tests was 53, which is significantly lower than the 434 eRNAs we have identified.

Given that lncRNAs are expressed in a highly cell-type and spatiotemporally specific manner (Mercer et al., 2008; Deveson et al., 2017), we next considered the mechanisms underlying the cell-type-specific and state-dependent expression of learning-induced lncRNAs. Open chromatin accessibility sites were compared with publicly available data on H3K27^{ac}, H3K4^{me1}, and CREB binding protein (CBP) occupancy in the adult brain that occurs following behavioral training (Halder et al., 2016). In Arc+ RC mice, among the 60,962 significant chromatin accessibility sites, we found that 25.2% (5,915) of all lncRNAs detected were associated with open chromatin, with 2,718 regions exhibiting features of active enhancers following fear-related learning (Figure S2). In the Arc+ neurons of EXT mice, a total of 51,673 peaks was detected by ATAC-seq, with 23.2% (5,460) of all lncRNAs being associated with increased chromatin accessibility. We found 2,501 regions that exhibited features of active enhancers associated with fear extinction learning (Table S1). Together, these data show that the active regulation of numerous lncRNAs in response to learning is associated with markers of enhancer activity and suggest that the experience-dependent expression of lncRNA in the adult brain may be more widespread than currently appreciated.

A significant population of enhancer-derived lncRNAs that are induced by fear extinction learning correlate with proximal protein-coding gene expression

We next focused on lncRNAs that were associated with enhancers (termed eRNAs) using ATAC-seq, as well as the publicly available CBP, H3K27^{ac}, and H3K4^{me1} signatures. We identified 434 putative eRNAs in Arc+ EXT neurons that overlapped with all four enhancer markers (Figure 1C). In mRNAs positioned downstream of these eRNAs, we observed less variability in expression within Arc+ EXT-activated neurons compared with quiescent Arc− EXT neurons derived from the same brain region (Figure 1D). A gene ontology (GO) analysis was then performed to explore the putative functional networks of protein-coding genes positioned proximal to eRNAs expressed during fear extinction learning. We found that these genes were most significantly enriched for GOs linked to “cytoplasmic vesicle membrane,” “neuron to neuron synapse,” “vesicle membrane,” and “synaptic membrane” (Figure 1E; Table S1). Other significant GO terms that contained fewer transcripts but were nonetheless interesting in the context of fear extinction were “DNA repair,” “nuclear speckles,” and several vesicle-related or postsynaptic-related clusters.

Six candidate proximal lncRNA:mRNA pairs were next selected for qPCR validation (Figures 2A–2F) based on the diversity of their genomic organization, their variable length (600–3,000 nt), and the fact that their associated protein-coding genes have previously been shown to be involved in neuronal plasticity and/or memory-related processes (Gross et al., 2015; Shanmugam et al., 2018, Bjorge et al., 2015, Salatino-Oliveira et al., 2016, Cruceanu et al., 2016., McNulty et al., 2012). These include two known lncRNAs with bidirectional promoters (*Gm26559*:*Map1b*, *Gm17733*:*Syn2*), another known intergenic lncRNA (*A730063M14Rik*:*Agap2*), an antisense lncRNA (*Gm15492*:*Ogg1*), and two functionally uncharacterized transcripts (*Gm13830*:*Srsf9 and BB557941*:*Nr4a2*). In each

case, we observed a positive relationship between the expression of the lncRNA and its proximal protein-coding mRNA, as determined by qPCR, and four of the six targets showed strong positive correlations ($r > 0.75$, Figures 2A–2F and S3; Table S2). The discrepancy between the lncRNA capture-seq results and the qPCR findings likely stems from the fact that qPCR focuses solely on a single exon, whereas sequencing provides an average of read coverage across the entire transcript, which then undergoes a more stringent statistical test in order to counteract the problem of multiple testing. Indeed, an examination of the read pile-up across the ADRAM locus suggests that there are more transcripts associated with the third exon, which is specifically targeted by our PCR primer design. Taken together, our data provide further evidence that there is a positive relationship between inducible eRNAs and downstream protein-coding RNA expression. A series of recent studies demonstrated that eRNA expression in neurons is associated with their proximity to plasticity-related protein-coding genes. Carullo et al. (2020) found that eRNA expression correlated more strongly with proximal genes than with distal genes by filtering transcriptionally active putative enhancers and protein-coding gene pairs from their RNA-seq and ATAC-seq data. Furthermore, using a candidate approach, they also demonstrated that an eRNA proximal to the Fos gene was sufficient to drive Fos mRNA expression. In another study, targeted shRNA knockdown of an eRNA proximal to the Arc gene promoter specifically blocked Arc mRNA induction (Schaukowitch et al., 2014). In addition, eRNA transcribed from the Npas4 enhancer region (~3 kb upstream of the TSS) plays an important role in the regulation of Npas4 mRNA expression (Hughes et al., 2021). Given that Nr4a2 is an immediate-early gene, such as Fos, Arc, and Npas4, and is directly involved in learning and memory (McNulty et al., 2012; Chatterjee et al., 2020), we subsequently focused our investigation on the mechanistic relationship between its proximal lncRNA *BB557941* (Figure 2G), which we have named *ADRAM*, and the epigenomic regulation of *Nr4a2* within the context of fear extinction.

Learning-induced *ADRAM* expression is necessary for the induction of the immediate-early gene *Nr4a2* and is required for fear extinction memory

The enhancer-derived lncRNA ADRAM (NONCODE TRANSCRIPT: NONMMUT037361.2), contains three exons and is 1,099 bp in total length, which is transcribed from a region 7 kb upstream of the Nr4a2 TSS. According to the NONCODE database (http://www.noncode.org/index.php), ADRAM is expressed in the cortex, hippocampus, spleen, and thymus but not in the liver, lung, or heart. As *ADRAM* and *Nr4a2* are both up-regulated in the ILPFC response to fear extinction learning, we investigated whether *ADRAM* expression is necessary for the induction of the *Nr4a2*. First, using fluorescence *in situ* hybridization, we determined that ADRAM is selectively expressed in the nucleus of the cortical pyramidal neurons *in vitro* (Figure S4). Next, in order to elucidate its functional role in fear extinction, ASOs were used to knock down ADRAM expression *in vivo*. Three different ASOs targeting *ADRAM* were first tested on primary cortical neurons, *in vitro* (Figure S5). ASO1 exhibited the best knockdown efficiency (at 200 nM). Injection of ASO1 into ILPFC neurons prior to fear extinction training (Figure S5) resulted in a significant reduction in learning-induced *ADRAM* expression (Figure 3A) and blocked the induction of *Nr4a2* mRNA expression (Figure 3B). Importantly, knocking down *ADRAM* prior to fear extinction training (Figure 3C) had

no effect on within-session performance during extinction training (Figure 3D), and there was also no effect of ADRAM knockdown on fear expression in RC mice (Figure 3E). In contrast, a significant impairment in fear extinction memory was observed in EXT mice trained in the presence of *ADRAM* knockdown (Figure 3E), with no effect on anxiety-like behavior in the open-field test (Figure S5). Together, these data demonstrate a necessary role for ADRAM in regulating Nr4a2 expression and the formation of fear extinction memory, which is clearly the result of an effect on cognition and memory that is independent of an effect on anxiety-like behavior.

ADRAM regulates the induction of the immediate-early gene Nr4a2 via a direct interaction with the *Nr4a2* promoter

A substantial proportion of lncRNAs were identified as putative eRNAs based on the observation that they are transcribed from open chromatin regions of the genome and share $H3K27^{ac}$, $H3K4^{me1}$, and CBP features of enhancer elements. eRNAs are known to be critical for regulating adjacent protein-coding gene expression (Kim et al., 2015a,b), although enhancer elements themselves can influence proximal gene expression through dynamic changes in the three-dimensional architecture of the genome (Wang et al., 2019). We therefore asked if the *ADRAM* lncRNA forms a tether with the *Nr4a2* promoter through chromatin looping. Chromatin conformation capture (3C) (Hagege et al., 2007) was used to analyze the organization of the chromatin environment by quantifying the physical interaction between the enhancer region that encodes *ADRAM* and the *Nr4a2* gene promoter. This analysis revealed no significant change in chromatin conformation after EXT, relative to RC (Figure 4A and S6), indicating that ADRAM does not coordinate the induction of Nr4a2 mRNA expression in response to fear extinction learning via a long-distance DNA-DNA interaction.

Given that eRNAs can form R-loops, which then serve to promote gene expression (Cloutier et al., 2016), we also considered the possibility that *ADRAM* forms an lncRNA:DNA hybrid, which could interact with the *Nr4a2* gene locus and regulate mRNA transcription in response to fear extinction training. To determine whether there is an R-loop structure around the TSS of the *Nr4a2* promoter, we used a DNA-RNA immunoprecipitation (DRIP) assay using S9.6 antibody, which recognizes R-loops. DRIP-qPCR targeting the TSS revealed no difference between RC and EXT mice (Figure 4B). The effect of fear extinction learning on the occupancy of the R-loop reader protein GADD45a (Arab et al., 2019) at the same site within the *Nr4a2* promoter was also examined and, again, no evidence of R-loop formation in response to extinction training was observed (Figure 4C). Therefore, we conclude that *ADRAM* does not form R-loops to coordinate fear extinction learning-induced *Nr4a2* mRNA expression.

Finally, to determine whether the *ADRAM* lncRNA interacts with the *Nr4a2* gene promoter, we used chromatin isolation by RNA purification (ChIRP) (Chu et al., 2015). We found that *ADRAM* binds directly to the *Nr4a2* promoter at a specific site ~500 bp upstream of the TSS (Figures 4D and S7), which was associated with an increase in the accumulation of the histone modification $H3K4^{me3}$, a marker of gene activation (Figure 4E). Critically, this effect was blocked in the presence of ASO-mediated ADRAM knockdown (Figure S7).

These findings strongly suggest that there is a physical interaction between *ADRAM* and the *Nr4a2* promoter, and that this is associated with the induction of an active chromatin state.

ADRAM serves as both a guide and a scaffold to coordinate fear extinction learning-induced Nr4a2 mRNA expression

LncRNAs are known to act as guides and scaffolds that recruit transcription factors and chromatin-modifying enzymes to specific gene loci. To determine whether the *ADRAM* lncRNA functions as a guide for transcriptional factors, we sought to identify the proteins that interact with *ADRAM* in response to fear extinction learning. To investigate this, we performed ChIRP followed by mass spectrometry to provide a comprehensive profile of proteins that bind to the ADRAM lncRNA, and which could then be recruited to the *Nr4a2* promoter in response to fear extinction learning. In RC mice, the most abundant interacting protein was the adhesion molecule γ-catenin, which has been shown to be a core component of the blood-brain barrier (Figure 5A; Table S3). Notably, beyond structural proteins in the nucleus, such as β-actin, the chaperone protein *14-3-3* was identified as one of the top proteins to interact with the *ADRAM* lncRNA in EXT nice (Figures 5B; Table S3). The 14-3-3 family is highly conserved, enriched in the brain, and plays an important role in the intracellular localization of target proteins (Giles et al., 2003; Zhang and Zhou, 2018). Therefore, we validated the interaction between ADRAM and 14-3-3 by formaldehyde-RNA immunoprecipitation (Figure 5C). We then used chromatin ChIRP analysis to examine whether 14-3-3 physically interacts with the N4ra2 promoter, revealing that this interaction is under temporal control. 14-3-3 interacts with the Nr4a2 promoter immediately after extinction training without a change in the level of 14-3-3 protein expression (Figure S8), an interaction that is reduced 1 h later (Figure 5D). These results confirm a functional role for 14-3-3 in the brain and provide evidence to suggest that the 14-3-3 chaperone also acts as a temporally regulated RNA-binding protein in the brain during fear extinction learning, and that 14-3-3 is directed to the Nr4a2 promoter by ADRAM in a learning-dependent manner.

We next explored the functional consequences of the activity-dependent recruitment of 14-3-3 to the Nr4a2 promoter on the epigenomic regulation of Nr4a2 gene expression. Given the critical role of HDAC3 and HDAC4 as negative regulators of learning and memory (McQuown et al., 2011; Sando et al., 2012; Zhu et al., 2019), we first questioned whether there are dynamic changes in HDAC occupancy in response to fear extinction learning. There was a time-dependent reduction in the presence of both HDAC3 (Figure 6A) and HDAC4 (Figure 6B) at the Nr4a2 promoter following fear extinction training. It is well established that the histone acetyltransferase CBP facilitates CREB activity at the *Nr4a2* promoter, which also leads to increased *Nr4a2* mRNA expression in response to various forms of learning (Bridi et al., 2017), although the mechanism by which CBP is selectively recruited has never been revealed. We found that CBP occupancy was increased at the *Nr4a2* promoter following fear extinction learning (Figure 6C). Following these observations, we explored whether the effect of extinction learning on HDAC3, HDAC4, and CBP occupancy at the Nr4a2 gene promoter is due, in part, to a role of ADRAM as a scaffold for 14-3-3. Previous work has shown that the phosphorylation-dependent binding of 14-3-3 to HDAC4 serves to regulate its nuclear activity by sequestering HDAC4 from the nucleus into the cytoplasm in a signal-dependent manner (McKinsey et al., 2000; Wakeling et al., 2021).

To confirm a scaffolding role for ADRAM, an infusion of ASO into the ILPFC was used to knock down *ADRAM* expression, which blocked the expulsion of HDAC3 and HDAC4 and inhibited the accumulation of CBP at the Nr4a2 promoter (Figures 6D–6F). These results suggest that *ADRAM* guides 14-3-3 to the Nr4a2 promoter, which results in the time-dependent removal of HDAC3 and HDAC4, followed by the coordinated deposition of CBP. Together with the establishment of an active chromatin state in response to extinction learning, our findings confirm previous observations of a tight relationship between HDAC3, HDAC4, and CBP in the epigenomic regulation of immediate-early gene expression and support a model whereby an eRNA-mediated mechanism drives the activation of *Nr4a2* in response to fear extinction learning (Figure 6G). As ADRAM is also expressed in other brain regions, including the hippocampus, cerebellum, and somatosensory cortex (Figure S9), it is likely that this eRNA is more generally involved in the regulation of experience-dependent Nr4a2 expression and in other memory processes. However, given that we did not observe a relationship between ADRAM and Nr4a2 in female mice, Nr4a2 may also be regulated by other molecular mechanisms, which could occur in a sex-specific manner (Figure S9).

Nr4a2 expression is necessary for the formation of fear extinction memory

Finally, given the causal effect of *ADRAM* as a guide and scaffold to coordinate the regulation of extinction-learning-induced *Nr4a2* mRNA expression, we wished to determine whether *Nr4a2* itself is critical for the formation of fear extinction memory. We first generated *Nr4a2* lentiviral shRNA plasmids and validated them in N2A cells (Figure S10), as well as verifying transfection efficiency *in vivo* (Figures 7A and 7B). Infusion of the *Nr4a2* knockdown construct into the ILPFC prior to fear extinction training (Figure 7C) had no effect on within-session extinction training (Figure 7D). There was a significant impairment in fear extinction memory (Figure 7E) with no influence on the ability to express fear. Similar to the observed effect with the ADRAM knockdown, Nr4a2 shRNA-treated mice exhibited normal anxiety-like behavior (Figure S10). These data demonstrate that the effect of Nr4a2 knockdown on fear extinction is due to its influence on cognition rather than on non-specific physiological indicators of generalized anxiety. We therefore conclude that ADRAM is required for the learning-induced regulation of Nr4a2, with our findings revealing a necessary role for the immediate-early gene Nr4a2 in the formation of fear extinction memory.

DISCUSSION

Here, we report the discovery of widespread experience-dependent lncRNA activity in the adult ILPFC, and further reveal a significant number of inducible eRNAs that respond selectively to fear extinction learning. This class of lncRNA was first discovered at scale more than a decade ago by the Greenberg group who identified thousands of sites outside known promoter regions in primary cortical neurons stimulated with KCl *in vitro*, which exhibited features of enhancer elements, including binding of CBP and the deposition of the histone modification $H3K4^{me1}$ (Kim et al., 2010). Transcriptional activity at these sites showed a positive correlation with downstream mRNA expression, suggesting a context-specific permissive relationship between eRNAs and their proximal mRNA partners.

Malik et al. (2014) went on to functionally characterize neuronal enhancers and identify another histone modification, H3K27^{ac}, as a key marker of their active state. An overlay of our lncRNA capture-seq data with learning-induced enhancer signatures in the adult brain (Halder et al., 2016), as well as our cell-type-specific ATAC-seq signatures in learning-activated Arc+ neurons, revealed that there are many experience-dependent lncRNAs in the ILPFC that are endowed with features of activity-inducible eRNAs. Notably, all six of the validated eRNA-associated protein-coding gene candidates have been shown to be involved in plasticity, suggesting that this class of lncRNA is, in general, permissively involved in the regulation of experience-dependent gene expression.

One of the most interesting findings of our study beyond the necessary role of ADRAM in fear extinction is that it binds directly to the Nr4a2 promoter; however, in doing so it does not form an R-loop or promote chromosome looping. *trans*-Acting lncRNAs are known to form triplex structures on double-stranded DNA using a Hoogsteen base-pairing rule in the DNA target (Li et al., 2016). These structures are distinct from R-loops and could represent a mechanism by which lncRNAs act in a combinatorial manner to simultaneously serve as both guides and scaffolds. Indeed, examination of the 1 kb upstream promoter sequence of NR4A2 revealed two sites proximal to the TSS, with 25 nucleotide long complementary sequences found within exon III of ADRAM. Notably, these sites overlap with G-quadruplex motifs that are predicted to enable triplex formation. These findings suggest that ADRAM functions as a guide via a direct interaction with the Nr4a2 promoter and may do so via the formation of an RNA:DNA triplex at sites of structural reactivity. Future studies will investigate whether dynamic DNA structure states are the key to how lncRNAs find their genomic targets to regulate gene expression in an experience-dependent manner.

The 14-3-3 family of evolutionarily conserved chaperone proteins is ubiquitously expressed in the brain and highly enriched at the synapse (Martin et al., 1994) being involved in a variety of neuronal processes, including synaptic plasticity (Berg et al., 2003; Marzinke et al., 2013; Foote et al., 2015). Our discovery of a direct interaction between ADRAM and 14-3-3 extends the capabilities of this class of chaperones to include functional activity as both an RNA-binding protein and a molecule that exerts its influence through protein-protein interactions. This is not without precedent as many proteins are able to interact with RNA, DNA, and other proteins. For example, YY1 interacts with both RNA and DNA, as well as other proteins, to promote its role as a regulator at the Xist locus (Jeon and Lee, 2011). Together with the observation that 14-3-3 is involved in learning and memory (Qiao et al., 2014), and our demonstration of how 14-3-3 interacts with eRNA to facilitate gene expression in fear extinction, these findings advance our understanding of the functional importance of this class of chaperones in the brain.

Histone modifications at neuronal enhancers also appear to be a requirement for the induction of activity-dependent genes and are particularly important in the case of rapidly induced immediate-early genes (Chen et al., 2019). We found a broad overlap with H3K27^{ac}, an open chromatin ATAC signature in activated neurons, and the expression of lncRNAs. Previous work has shown that eRNA activity often precedes, and then drives, the expression of immediate-early genes, such as c-Fos, which occurs via a direct interaction with the histone acetyltransferase domain of CBP (Carullo et al., 2020). In addition, a large

number of eRNAs have been shown to bind to CBP, correlating with the expression of downstream genes that require CBP for their induction (Bose and Borger, 2017). Our data on the functional relationship between ADRAM, HDAC3, HDAC4, CBP, and Nr4a2 agree with these observations and, importantly, extend the findings to include the ILPFC where they are critically involved in fear extinction. Our conclusion is that ADRAM functions as both a guide and a scaffold to epigenomically regulate extinction learning-induced Nr4a2 expression. There are now many examples of multifunctional lncRNAs. For example, in dopaminergic neurons, antisense Uchl1 regulates the expression of Uchl1 in the nucleus and then shuttles to the cytoplasm where it promotes Uchl1 translation (Carrieri et al., 2012). Furthermore, owing to its modular domain structure, Neat1 functions in *cis* to coordinate the deposition of learning-related repressive chromatin modifiers along the genome (Butler et al., 2019) and in *trans* to govern paraspeckle assembly by influencing phase separation (Yamazaki et al., 2018).

In summary, the discovery of an lncRNA that is required for fear extinction deepens our understanding of learning-induced epigenomic mechanisms by integrating the modular function of enhancer-derived lncRNAs with key epigenomic processes involved in memory, and answers the long-standing question of how certain HDACs and CBP coordinate to confer their influence on localized gene regulation with a high degree of state-dependent selectivity. LncRNAs therefore provide a bridge to link dynamic environmental signals with epigenomic mechanisms of gene regulation. Together, these findings broaden the scope of experience-dependent lncRNA activity, and underscore the importance of considering eRNAs in the adult cortex as potential therapeutic targets for fear-related neuropsychiatric disorders.

Limitations of the study

In this work, we identify an enhancer-derived lncRNA that is necessary for the formation of fear extinction memory in male mice. However, an examination of ADRAM and Nr4a2 mRNA expression in the ILPFC after extinction learning in randomly cycling females revealed no increase in ADRAM expression in the female ILPFC. In contrast, Nr4a2 was induced by training in both males and females (Figure S9). These results indicate that, although Nr4a2 may be generally induced by experience in both sexes, it may not be regulated by ADRAM under conditions where successful extinction does not occur. With respect to sex differences in fear extinction, we have also previously found that male and female mice respond differently to the standard extinction protocol used in our laboratory (Baker-Andresen et al., 2013) and that the electrophysiological signature in the prelimbic PFC during fear extinction is very different between males and females (Fenton et al., 2014, 2016). Therefore, it is highly plausible that there are female-specific molecular mechanisms that are involved in fear-related learning. Future studies on the role of lncRNAs in fear extinction in females will require the use of a sex-specific learning protocol to reveal brain region-specific molecular mechanisms underlying memory in these mice. In addition, although we have demonstrated that 14-3-3 is a key regulatory protein that interacts with ADRAM, there were other candidates identified by mass spectrometry that have not been validated. At this stage, these data should therefore be considered preliminary until further

experiments are carried out. Finally, it is not yet known whether ADRAM is necessary for other forms of learning.

STAR★METHODS

RESOURCE AVAILABILITY

Lead contact—Further information and requests for resources and reagents should be directed to and will be fulfilled by Timothy W. Bredy (t.bredy@uq.edu.au).

Materials availability—All unique/stable reagents generated in this study are available from the Lead Contact upon reasonable request.

Data and code availability

- The data analysis pipeline and customized PERL scripts are available through the GitHub page (https://github.com/Qiongyi/lncRNA_2020). All the sequencing data are publicly available Database: GSE181706. In addition, we have also made our custom tracks publicly available via the UCSC genome browser with the link (http://genome.ucsc.edu/cgi-bin/hgTracks?db=mm10&hubUrl=https://data.cyverse.org/dav-anon/iplant/home/qiongyi/lncRNA2020/hub_lncRNA2020_v1.0.txt).
- This paper does not report original code.
- Any additional information required to reanalyze the data reported in this paper is available from the lead contact upon request.

EXPERIMENTAL MODEL AND SUBJECT DETAILS

Animals—10–12-week-old C57BL/6 male and female mice were housed in same sex groups, four per cage, maintained on a 12 h light/dark time schedule, and allowed free access to food and water. All experiments took place during the light phase in red-light-illuminated testing rooms following protocols approved by the Animal Ethics Committee at the University of Queensland.

Primary cortical neuron, N2A and HEK293T cell culture—Pregnant female C57BL/6 mice were euthanized at E16, and embryos immediately collected in ice-cold PBS. Embryonic cortices were dissected and enzymatically dissociated with 5 U/mL papain at 37°C for 20 min. Papain was washed out with neuronal culture medium (Neurobasal medium supplemented with 1% GlutaMAX and 2% B-27). The dissociated cells were passed through a 40 μm cell strainer (BD Falcon) and plated onto 6-well plates coated with poly-L- ornithine (Sigma P2533) at a density of 1×10^6 cells per well. Neuronal cultures were maintained in an incubator at 37°C with 5% CO_2. The culture medium was replaced 24–48 h after preparation of the cultures, and thereafter medium was changed every third day by replacement of 50% of the total volume. N2a cells were maintained in medium containing half DMEM, high glucose (Gibco), half OptiMEM 1 (Gibco) with 5% serum and 1% Pen/Strep. HEK293T cells were maintained in medium contains DMEM, high glucose (Gibco) with 5% serum and 1% Pen/Strep.

METHOD DETAILS

DNA/RNA extraction—Tissue derived from the infralimbic prefrontal cortex (ILPFC) of Retention Control (RC) or Extinction (EXT) trained mice was homogenized using a Dounce tissue grinder in 500 μL of cold 1X DPBS (Gibco). 400 μL of homogenate was used for DNA extraction, and 100 μL was used for RNA extraction. DNA extraction was carried out using the DNeasy Blood & Tissue Kit (Qiagen), and RNA was extracted using Trizol (Invitrogen). Both extraction protocols were followed according to the manufacturer's instructions. The concentration of DNA and RNA was measured by Qubit assay (Invitrogen).

Quantitative RT-PCR—A total of 500 ng RNA was used for cDNA synthesis using the PrimeScript Reverse Transcription Kit (Takara). Quantitative PCR was performed on a RotorGeneQ (Qiagen) cycler with the Rotor-Gene SYBR Green PCR Kit (Qiagen) by using primers for target genes and PGK1 as an internal control (Table S4). The ΔΔCT method was used for analysis, and each PCR reaction was run in duplicate for each sample and repeated at least twice.

Lentiviral Nr4a2 knockdown—Lentiviral plasmids were generated by inserting either Nr4a2 shRNA or scrambled control (Table S4) fragments in a modified FG12 vector (FG12H1, derived from the FG12 vector originally provided by David Baltimore, CalTech) as previously described (Li et al., 2019). Lentivirus was prepared and maintained according to protocols approved by the Institutional Biosafety Committee at the University of Queensland. Briefly, HEK293 T cells were grown to 70% confluence in triple-layer flasks. Lipofectamine 2000 was used to transfect cells with the plasmids pMDG, pRSV-rev and pMDLg/pRRE and the transfer vector (Nr4a2 or control shRNA cloned into FG12). Transfected cells were cultured for 48 h, after which the culture medium was collected, clarified, filtered, and lentivirus particles concentrated by ultracentrifugation. Concentrated viral pellets were resuspended in PBS and snap-frozen.

Cannulation surgery and lentiviral infusion—A double cannula (PlasticsOne) was implanted in the anterior posterior plane, +/− 30° along the midline, into the ILPFC. The coordinates of the injection locations were centred at +1.80 mm in the anterior-posterior plane, and −2.7 mm in the dorsal-ventral plane. Mice were first fear conditioned, followed by 2x Antisense oligonucleotide or lentiviral infusions (24 h post fear conditioning and, after 7 days, they were extinction trained.

Behavioral training—Two contexts (A and B) were used for all behavioral testing. Both conditioning chambers (Coulbourn Instruments) had two transparent walls and two stainless steel walls with a metal grid floor (3.2 mm in diameter, 8 mm center). The floors in context B were covered with a flat white plastic non-transparent surface with two white LED lights used to minimize context generalization. Individual digital cameras were mounted on the ceiling of each chamber and connected via a quad processor for automated scoring of freezing behavior (FreezeFrame). Fear conditioning was performed in context A using a 120 s pre-fear conditioning period, followed by three pairings of a 120 s, 80dB, 16kHZ pure tone conditioned stimulus (CS) co-terminating with a 1 s (2 min intervals), 0.7 mA foot shock

(US). Mice were counterbalanced into equivalent treatment groups based on freezing during the third training CS. For extinction (EXT), mice were placed in context B and acclimated for 2 min. Then, extinction training comprised 30 non-reinforced 120 s CS presentations (5-s intervals). For retention control (RC), fear conditioned mice were exposed to context B for an equal amount of time but without non-reinforced CS exposure. For the retention test, all mice were returned to context B and following a 2 min acclimation (used to minimize context generalization), freezing was assessed during three 120 s CS presentations (120 s intertrial interval). Memory was calculated as the percentage of time spent freezing during the test.

Open-field test—Mice were tested in the open field to assess generalized anxiety or reduced spontaneous locomotion. The open-field test was conducted in a sound-attenuated, dimly illuminated with white lighting (60 ± 3 lux) room. Mice were placed into the center of a white plastic open field (30 × 30 × 30 cm) and movement was recorded with an overhead camera for 20 min. Videos were analyzed using Noldus EthoVision 11 to determine the distance traveled, and the number of entries into and cumulative time spent in the center of the arena (defined as a 15 × 15 cm square concentric with the base of the arena).

Behavioral training (for tissue collection)—Immediately after EXT or RC training the ILPFC was collected by targeted micropunch based on the Paxinos and Watson mouse brain atlas per our previous studies (Lin et al., 2011; Wei et al., 2012; Li et al., 2014, 2019; Marshall et al., 2020).

Immunohistochemistry—Mice were euthanized with 100 mg/kg ketamine mixed with 10 mg/kg xylazine, after which they were perfused with 60 mL PBS followed by 4% paraformaldehyde in PBS. Following extraction, the brains were stored in 4% paraformaldehyde overnight. The brains were then placed in 30% sucrose for a minimum of 24 h prior to cryostat slicing. Sectioning at 40 μm was performed using CM1950 cryostat (Leica), and sections were mounted on Superfrost Plus microscope slides (Fisher Scientific). The sections were incubated 1–2 h in blocking buffer, after which primary antibodies (MAP2 or GFP, Table S4) were added and the slides incubated at 4°C overnight. The slides were then washed 3 times with PBS containing 0.02% Tween 20 (PBS-T), after which secondary antibodies were added (Dylight 488-conjugated AffiniPure sheep anti-goat IgG or Dylight 549-conjugated AffiniPure goat anti-rabbit IgG, Jackson ImmunoReasearch Laboratories). The slides were incubated at room temperature for 45 min, washed 3 times with PBST and sealed with Prolong Diamond Antifade Mountant (Life Technology).

Fluorescence *in situ* hybridization—Custom Stellaris® FISH Probes (Table S4) were designed against ADRAM using the Stellaris® FISH Probe Designer (Biosearch Technologies). The cultured primary neurons and adult mouse brain sections were hybridized with the ADRAM Stellaris FISH Probe set labeled with TAMRA (Biosearch Technologies, Inc.), following the manufacturer's instructions.

Chromatin immunoprecipitation—Chromatin immunoprecipitation (ChIP) was performed following a modification to the Invitrogen ChIP kit protocol. ILPFC samples were fixed in 1% formaldehyde and cross-linked cell lysates were sheared by Covaris in 1%

SDS lysis buffer to generate chromatin fragments with an average length of 300 bp using peak power: 75, duty factor: 2, cycle/burst: 200, duration: 900 s and temperature: between 5°C and 9°C. The chromatin was then immunoprecipitated using the specific antibody to each target. An equivalent amount of control normal rabbit IgG (Santa Cruz) was used as a non-specificity control and the sample was incubated overnight at 4°C. Protein-DNA-antibody complexes were precipitated with protein G-magnetic beads (Invitrogen) for 1 h at 4°C, followed by three washes in low salt buffer, and three washes in high salt buffer. The precipitated protein-DNA complexes were eluted from the antibody with 1% SDS and 0.1 M $NaHCO_3$, then incubated for 4 h at 60°C in 200 mM NaCl to reverse the formaldehyde cross-link. Following proteinase K digestion, phenol-chloroform extraction, and ethanol precipitation, samples were subjected to qPCR using primers (Table S4) specific for 200 bp segments within corresponding target regions.

Western blot—Protein samples were extracted using NP40 solution following the manufacturer's protocol (Thermo Fisher) and the protein concentration was determined using the Qubit protein detection kit (Invitrogen), also following the manufacturer's protocol. Individual samples were run on a single 10-well gel pre-made 4–12% gel (Thermo Fisher). Briefly, samples were prepared on ice (to a final volume of 20 μL) and then vortexed and denatured for 10 min at 90°C. Gels were run with TBS-T and proteins were transferred onto a nitrocellulose membrane (Biorad). The membrane was blocked by blocking buffer (LI-COR) for 1 h at room temperature, washed with TBS-T for 5 min (three times) and incubated with 5 mL of 14-3-3 β/α and β-tubulin (control) antibodies (Table S4) in blocking buffer (LI-COR) overnight at 4°C. The membranes were washed with TBS-T (three times), incubated for 1 h with anti-mouse secondary antibody (1:15,000; LI-COR) and anti-rabbit secondary antibody (1:15,000; LI-COR) in blocking buffer (LI-COR), then washed with TBS-T for 10 min (three times) and 20 min (once). Absorbance readings of the membrane were taken using a LI-COR FX system following the manufacturer's protocol.

ASO knockdown ADRAM, *in vitro*—200 nM of ADRAM ASO or scrambled control (Table S4) was dropped onto primary cortical neurons in a 6-well plate. After 7days *in vitro*, the cells were harvested for RNA extraction.

Fluorescence-activated cell sorting (FACS)—Frozen ILPFC tissue samples were homogenized and fixed with 1% methanol-free PFA (Thermo Fisher) at room temperature for 5 min. Glycine, at a final concentration of 0.125 mM was used to stop the fixation reaction. The cells were then washed three times with cold PBS. The cell suspension was treated with DNaseI (Thermo Fisher) for 15 min at 4°C, followed by a wash step with 1 mL of cold PBS. The cell suspension was then blocked using FACS blocking buffer (BSA, normal Goat Serum and 1% Triton X-100) for 15 min at 4°C with end-to-end rotation. After 15 min blocking, the cell suspension was incubated with 1:1000 dilution of pre-conjugated Arc antibody (Bioss) and 1:2000 dilution of pre-conjugated NeuN antibody (Abcam) at 4°C for 1 h with an end-to-end rotation. At the end of incubation, two rounds of 1 mL 1X cold PBS washes were applied. The cell pellets were resuspended with 500 μL of cold PBS, and a 1:2000 dilution of DAPI was added. FACS was performed on a BD FACSAriaII

(BD Science) sorter within the Flow Cytometry Facility at the Queensland Brain Institute, University of Queensland, Brisbane.

Long noncoding RNA capture sequencing—ILPFC tissue was collected immediately after RC or EXT training (N = 24). 2 μg of total RNA isolated from ILPFC tissue (4 pooled per library, 3 libraries per group) was used to generate the RNA library. Total RNA was treated using a NEBNext® rRNA Depletion Kit (NEB) to remove rRNA. RNA libraries were then generated using a NEBNext® Ultra™ II RNA Library Prep Kit for Illumina® (NEB). A custom-designed probe panel (Roche), which targets 28,228 known and predicted mouse lncRNAs (Bussotti et al., 2016), was used to capture lncRNAs in accordance with the SeqCap EZ Hybridization and Wash Kit and SeqCap EZ Accessory Kit (Roche). Briefly, 1 μg of RNA library was mixed with 5 μL of 1 mg/mL COT DNA and dried in a DNA vacuum concentrator at 60°C. To each dried-down amplified sample library/COT DNA, 7.5 μL of Hybridization Buffer and 3 μL of Hybridization Component A was added, then put onto a 95°C heat block for 10 min to denature the DNA. 4.5 μL of lncRNA probes was then added to the denatured library and incubated in a thermocycler at 47°C for 72 h. After hybridization, 100 μL Streptavidin Dynabeads was added to the tube. The captured sample was then bound to the beads by placing the tubes containing the beads and DNA in a thermocycler set to 47°C for 45 min. The captured sample was then washed with wash buffer I, stringent wash buffer, wash buffer II and wash buffer III, provided in the kit. Captured lncRNA libraries were sequenced on an Illumina HiSeq 4000 platform with a read length of 150 bp × 2.

Assay for transposase-accessible chromatin using sequencing (ATAC-seq)—Male mice (N = 30) were either RC (n = 15) of EXT (n = 15) trained and five ILPFCs were pooled for FACS. After FACS, Arc + NeuN+ and Arc-NeuN + populations from the RC or EXT group (n = 3 libraries per pooled group) were used for ATAC-seq according to the following procedure. 50,000 cells were resuspended in 50 μL lysis buffer (20 mM Tris-HCl, pH 7.4; 20 mM NaCl; 6 mM $MgCl_2$; 0.10% Igepal CA-630) and spun down immediately (500 g for 10 min at 4°C). The transposase reaction was performed using the ATAC-seq kit (Active motif) following the manufacturers protocol. Briefly, the cell pellet was resuspended in 100 μL ice-cold ATAC lysis buffer, centrifuged and supernatant removed. Next, 50 μL of tagmentation master mix containing the assembled transposomes was added and incubated at 37°C for 30 min. Immediately following the tagmentation reaction, each sample was transferred to a clean 1.5 mL microcentrifuge tube and 250 μL DNA purification binding buffer and 5 μL 3 M sodium acetate was added to each sample. The samples were then purified using a DNA purification column and PCR amplified using i7 and i5 index primers to generate the ATAC-seq libraries. Paired-end (PE) libraries were sequenced using an Illumina HiSeq 4000 sequencing platform with a read length of 150 bp × 2.

Sequencing data analysis—Cutadapt (v1.17, https://cutadapt.readthedocs.io/en/stable/) was used to trim off low-quality nucleotides (Phred quality lower than 20) and Illumina adaptor sequences at the 3′ end of each read for both lncRNA capture sequencing (Capture-seq) and ATAC sequencing (ATAC-seq) data. Processed reads were aligned to the mouse reference genome (mm10) using HISAT2 (v2.1.0) (Kim et al., 2015a,b) and BWA-MEM

(0.7.17) (Li and Durbin, 2009) for Capture-seq and ATAC-seq data, respectively. SAMtools (version 1.8) (Li et al., 2009) was then used to convert “SAM” files to “BAM” files, remove duplicate reads, and sort and index the “BAM” files. To avoid artifact signals potentially introduced by misalignments, only properly PE aligned reads with a mapping quality of at least 20 were retained for downstream analyses. For Capture-seq data, three rounds of StringTie (v2.1.4) (Pertea et al., 2015) were applied to i) perform reference-guided transcriptome assembly by supplying the GENCODE annotation file (V25) with the “-G” option for each sample, ii) generate a non-redundant set of transcripts using the StringTie merge mode, and iii) quantify the transcript-level expression for each sample, with the option of “-e -G merged.gtf”. For the lncRNA analysis, known protein-coding transcripts (with the GENCODE transcript biotype as “protein-coding”) or transcripts with a length of less than 200 nt were removed from the StringTie results. Ballgown (v2.22.0) (Frazee et al., 2015) was then used to conduct transcript-level differential expression analysis.

For ATAC-seq data, BEDtools (v2.27.1) (Quinlan and Hall, 2010) was used to convert the BAM files to BED files. Reads aligned to the mitochondrial genome were discarded as the mitochondrial genome is more accessible due to the lack of chromatin packaging. To account for the 9 bp duplications created by DNA repair by Tn5 transposase, reads were shifted +4 bp and −5 bp for positive and negative strands, respectively. MACS2 (v2.2.4) (Zhang et al., 2008) was used for peak calling with the option of “–shift −75 –extsize 150 –nomodel -B –SPMR -g mm –keep-dup all”. One Arc + EXT sample was removed from the analysis due to extremely low sequencing quality. BEDtools with the “multiIntersectBed” function was used to identify the consistent peaks among biological replicates. Only consistent ATAC peaks detected in all biological replicates in at least one condition were collected and used for downstream analyses. We categorized ATAC peaks into different genomic categories using a custom PERL script. H3K27^{ac}, H3K4^{me1} and CBP data were downloaded from the NCBI GSE with the accession IDs “GSM1939159”, “GSM1939160”, “GSM1939127”, “GSM1939128” and “GSM530174”. For the CREB-binding protein (CBP) peaks, the genomic coordinates were converted from mm9 to mm10 using the liftOver script. LncRNAs containing each of the ATAC, H3K27^{ac}, H3K4^{me1} and CBP signatures were identified using a custom PERL script.

Quantitative analysis of chromosome conformation capture assay (3C-qPCR)—The 3C-qPCR protocol was adapted from a previous publication (Fullwood and Ruan, 2009). Briefly, ILPFC samples were harvested from either extinction trained or control mice and dissociated with cold PBS in a Dounce homogenizer to generate a cell suspension. Approximately 1.5 × 10^6 cells from each infralimbic prefrontal cortex were fixed with 1% formaldehyde for 10 min at room temperature and lysed, after which the nuclei were digested with DpnII (NEB) before ligation. All primers (Table S4) were designed within 150 bp from DpnII digestion site. The specificity and amplification efficiency of each primer were tested by performing qPCR on a serial dilution of the BAC clone (which contains the Nr4a2 locus) and generating a standard curve. Digestion efficiency, ligation efficiency, and sample purity were all verified as per established protocols. According to a (slope) and b (intercept) based on the standard curve of the BAC clone, we then transformed the values as 10^ (Ct-b)/a for each primer and normalized to GAPDH. The 3C quantitative results

are presented as the mean ± SEM from three independent preparations of 3C sample with duplicate qPCR data.

Chromatin isolation by RNA purification (ChIRP) analysis—ChIRP analysis was performed as previously described (Chu et al., 2015). Briefly, 1 mL of PBP (PBS and PIC) was combined with each ILPFC sample and gently homogenized and fixed in 3% formaldehyde solution for 30 min. The pellet was then resuspended with lysate buffer and incubated for 15 min on ice, then sheared using the Covaris M220. The oligonucleotide probe mix labeled with a biotin marker for ADRAM was added to the product and hybridized at 37°C for 4 h. Streptomycin biotin C1 protein beads were then added and incubated for 30 min, then washed for 3 times. Next, the magnetic beads were re-suspended in the biotin elution buffer (12.5 mM biotin, 7.5 mM HEPES [pH7.5], 75 mM NaCl, 1.5 mM EDTA, 0.15% SDS, 0.075% sarkosyl, and 0.02% Na-Deoxycholate) and, after shaking at room temperature for 20 min and 65°C for 10 min, the supernatant was removed, DNA extracted and qPCR using the primers (Table S4) amplifying the Nr4a2 promoter region.

Chromatin purification by RNA precipitation followed by mass spectrometry (ChIRP-MS)—Similar to ChIRP, after elution with the biotin elution buffer, the TCA precipitation method was used to extract protein for mass spectrometry to identify proteins associated with ADRAM.

HPLC/MS MS/MS analysis—Following the sample preparation method of Xiong et al., 2021, peptide extracts were analysed by nanoHPLC/MS MS/MS on an Eksigent ekspert nanoLC 400 system (SCIEX) coupled to a Triple TOF 6600 mass spectrometer (SCIEX) equipped with a PicoView nanoflow (New Objective) ion source. Full scan TOFMS data were acquired over the mass range 350–1800 and for product ion ms/ms 100–1500. Ions observed in the TOF-MS scan exceeding a threshold of 200 counts and a charge state of +two to + five were set to trigger the acquisition of product ion, ms/ms spectra of the resultant 30 most intense ions.

MS data analysis—Data were acquired and processed using Analyst TF 1.7 software (SCIEX). Protein identification was carried out using ProteinPilot software v5.0 (SCIEX) with the Paragon database search algorithm. MS/MS spectra were searched against the mouse proteome in the UniProt database (55,366 proteins). A non-linear fitting method was used to determine both a global and a local FDR from the decoy database search (Tang et al., 2008). The cut-off for identified proteins was set to 1% global FDR. The MS2Count was calculated for each identified protein by summing the MS2Count of all peptides belonging to that protein. The proteins identified using control probe were subtracted from the list of ADRAM-bound proteins, after which they were analyzed by STRING to determine functional protein association networks (https://string-db.org/).

QUANTIFICATION AND STATISTICAL ANALYSIS

All statistical analysis was performed using Prism 8. Following an analysis of descriptive statistics, a two-tailed unpaired Student’s t-test was used for direct comparisons between RC and EXT groups at each time point. One-way or two-way ANOVA was chosen for multiple

comparisons where appropriate. All post hoc analysis was performed using either Tukey's or Šídák's multiple comparison test where appropriate. Error bars represent SEM. Significant differences were accepted at $p < 0.05$.

Supplementary Material

Refer to Web version on PubMed Central for supplementary material.

ACKNOWLEDGMENTS

The authors gratefully acknowledge grant support from the Brain and Behavioral Research Foundation (NARSAD Independent Investigator Award, to T.W.B.), NIH R01MH109588 (to T.W.B. and R.C.S.), NIH 1R21MH103812 (to T.W.B.), ARC DP180102998 (to T.W.B.), ARC DP190100234 (to T.W.B.), NSFC 82171517 (to W.W.), and NSFC 82001421 (to X.L.). L.J.L., E.L.Z., and S.U.M. are supported by the Westpac Future Scholars and the University of Queensland. Imaging/analysis was performed at the Queensland Brain Institute's Advanced Microscopy Facility. We thank Mr. Alun Jones from the Institute for Molecular Biosciences Mass Spectrometry Facility for his technical support and Ms. Rowan Tweedale for helpful editing of the manuscript.

REFERENCES

Alberini CM (2009). Transcription factors in long-term memory and synaptic plasticity. Physiol. Rev 89, 121–145. 10.1152/physrev.00017.2008. [PubMed: 19126756]

Arab K, Karaulanov E, Musheev M, Trnka P, Schafer A, Grummt I, and Niehrs C (2019). GADD45A binds R-loops and recruits TET1 to CpG island promoters. Nat. Genet 51, 217–223. 10.1038/s41588-018-0306-6. [PubMed: 30617255]

Baker-Andresen D, Flavell CR, Li X, and Bredy TW (2013). Activation of BDNF signaling prevents the return of fear in female mice. Learn. Mem 20, 237–240. 10.1101/lm.029520.112. [PubMed: 23589089]

Barry G, Briggs JA, Vanichkina DP, Poth EM, Beveridge NJ, Ratnu VS, Nayler SP, Nones K, Hu J, Bredy TW, et al. (2014). The long non-coding RNA Gomafu is acutely regulated in response to neuronal activation and involved in schizophrenia-associated alternative splicing. Mol. Psychiatry 19, 486–494. 10.1038/mp.2013.45. [PubMed: 23628989]

Berg D, Holzmann C, and Riess O (2003). 14-3-3 proteins in the nervous system. Nat. Rev. Neurosci 4, 752–762. 10.1038/nrn1197. [PubMed: 12951567]

Bjorge MD, Hildrestrand GA, Scheffler K, Suganthan R, Rolseth V, Kusnierczyk A, Rowe AD, Vagbo CB, Vetlesen S, Eide L, et al. (2015). Synergistic actions of Ogg1 and mutyh DNA glycosylases modulate anxiety-like behavior in mice. Cell Rep. 13, 2671–2678. 10.1016/j.celrep.2015.12.001. [PubMed: 26711335]

Bose DA, and Berger SL (2017). eRNA binding produces tailored CBP activity profiles to regulate gene expression. RNA Biol. 14, 1655–1659. 10.1080/15476286.2017.1353862. [PubMed: 28891741]

Bredy TW, Wu H, Crego C, Zellhoefer J, Sun YE, and Barad M (2007). Histone modifications around individual BDNF gene promoters in prefrontal cortex are associated with extinction of conditioned fear. Learn. Mem 14, 268–276. 10.1101/lm.500907. [PubMed: 17522015]

Bridi MS, Hawk JD, Chatterjee S, Safe S, and Abel T (2017). Pharmacological activators of the NR4A nuclear receptors enhance LTP in a CREB/CBP-dependent manner. Neuropsychopharmacology 42, 1243–1253. 10.1038/npp.2016.253. [PubMed: 27834392]

Bruel-Jungerman E, Davis S, and Laroche S (2007). Brain plasticity mechanisms and memory: a party of four. Neuroscientist 13, 492–505. 10.1177/1073858407302725. [PubMed: 17901258]

Bussotti G, Leonardi T, Clark MB, Mercer TR, Crawford J, Malquori L, Notredame C, Dinger ME, Mattick JS, and Enright AJ (2016). Improved definition of the mouse transcriptome via targeted RNA sequencing. Genome Res. 26, 705–716. 10.1101/gr.199760.115. [PubMed: 27197243]

Butler AA, Johnston DR, Kaur S, and Lubin FD (2019). Long noncoding RNA NEAT1 mediates neuronal histone methylation and age-related memory impairment. Sci. Signal 12. 10.1126/scisignal.aaw9277.

Cabili MN, Dunagin MC, McClanahan PD, Biaesch A, Padovan-Merhar O, Regev A, Rinn JL, and Raj A (2015). Localization and abundance analysis of human lncRNAs at single-cell and single-molecule resolution. Genome Biol. 16, 20. 10.1186/s13059-015-0586-4. [PubMed: 25630241]

Cajigas I, Chakraborty A, Swyter KR, Luo H, Bastidas M, Nigro M, Morris ER, Chen S, VanGompel MJW, Leib D, et al. (2018). The Evf2 ultraconserved enhancer lncRNA functionally and spatially organizes megabase distant genes in the developing forebrain. Mol. Cell 71, 956–972.e959. 10.1016/j.molcel.2018.07.024. [PubMed: 30146317]

Carrieri C, Cimatti L, Biagioli M, Beugnet A, Zucchelli S, Fedele S, Pesce E, Ferrer I, Collavin L, Santoro C, et al. (2012). Long non-coding antisense RNA controls Uchl1 translation through an embedded SINEB2 repeat. Nature 491, 454–457. 10.1038/nature11508. [PubMed: 23064229]

Carullo NVN, Phillips RA Iii, Simon RC, Soto SAR, Hinds JE, Salisbury AJ, Revanna JS, Bunner KD, Ianov L, Sultan FA, et al. (2020). Enhancer RNAs predict enhancer-gene regulatory links and are critical for enhancer function in neuronal systems. Nucleic Acids Res. 48, 9550–9570. 10.1093/nar/gkaa671. [PubMed: 32810208]

Chanda K, Das S, Chakraborty J, Bucha S, Maitra A, Chatterjee R, Mukhopadhyay D, and Bhattacharyya NP (2018). Altered levels of long NcRNAs Meg3 and Neat1 in cell and animal models of Huntington's disease. RNA Biol. 15, 1348–1363. 10.1080/15476286.2018.1534524. [PubMed: 30321100]

Chatterjee S, Walsh EN, Yan AL, Giese KP, Safe S, and Abel T (2020). Pharmacological activation of Nr4a rescues age-associated memory decline. Neurobiol. Aging 85, 140–144. 10.1016/j.neurobiolaging.2019.10.001. [PubMed: 31732218]

Chen LF, Lin YT, Gallegos DA, Hazlett MF, Gomez-Schiavon M, Yang MG, Kalmeta B, Zhou AS, Holtzman L, Gersbach CA, et al. (2019). Enhancer histone acetylation modulates transcriptional bursting dynamics of neuronal activity-inducible genes. Cell Rep. 26, 1174–1188.e1175. 10.1016/j.celrep.2019.01.032. [PubMed: 30699347]

Chu C, Zhang QC, da Rocha ST, Flynn RA, Bharadwaj M, Calabrese JM, Magnuson T, Heard E, and Chang HY (2015). Systematic discovery of Xist RNA binding proteins. Cell 161, 404–416. 10.1016/j.cell.2015.03.025. [PubMed: 25843628]

Cloutier SC, Wang S, Ma WK, Al Husini N, Dhoondia Z, Ansari A, Pascuzzi PE, and Tran EJ (2016). Regulated formation of lncRNA-DNA hybrids enables faster transcriptional induction and environmental adaptation. Mol. Cell 62, 148. 10.1016/j.molcel.2016.03.012. [PubMed: 27058790]

Cruceanu C, Kutsarova E, Chen ES, Checknita DR, Nagy C, Lopez JP, Alda M, Rouleau GA, and Turecki G (2016). DNA hypomethylation of Synapsin II CpG islands associates with increased gene expression in bipolar disorder and major depression. BMC Psychiatry 16, 286. 10.1186/s12888-016-0989-0. [PubMed: 27515700]

Deveson IW, Brunck ME, Blackburn J, Tseng E, Hon T, Clark TA, Clark MB, Crawford J, Dinger ME, Nielsen LK, et al. (2018). Universal alternative splicing of noncoding exons. Cell Syst. 6, 245–255.e245. 10.1016/j.cels.2017.12.005. [PubMed: 29396323]

Deveson IW, Hardwick SA, Mercer TR, and Mattick JS (2017). The dimensions, dynamics, and relevance of the mammalian noncoding transcriptome. Trends Genet. 33, 464–478. 10.1016/j.tig.2017.04.004. [PubMed: 28535931]

Feng J, Shao N, Szulwach KE, Vialou V, Huynh J, Zhong C, Le T, Ferguson D, Cahill ME, Li Y, et al. (2015). Role of Tet1 and 5-hydroxymethylcytosine in cocaine action. Nat. Neurosci 18, 536–544. 10.1038/nn.3976. [PubMed: 25774451]

Fenton GE, Halliday DM, Mason R, Bredy TW, and Stevenson CW (2016). Sex differences in learned fear expression and extinction involve altered gamma oscillations in medial prefrontal cortex. Neurobiol. Learn Mem 135, 66–72. 10.1016/j.nlm.2016.06.019. [PubMed: 27344940]

Fenton GE, Pollard AK, Halliday DM, Mason R, Bredy TW, and Stevenson CW (2014). Persistent prelimbic cortex activity contributes to enhanced learned fear expression in females. Learn. Mem 21, 55–60. 10.1101/lm.033514.113. [PubMed: 24429423]

Foote M, Qiao H, Graham K, Wu Y, and Zhou Y (2015). Inhibition of 14-3-3 proteins leads to schizophrenia-related behavioral phenotypes and synaptic defects in mice. Biol. Psychiatry 78, 386–395. 10.1016/j.biopsych.2015.02.015. [PubMed: 25863357]

Frazee AC, Pertea G, Jaffe AE, Langmead B, Salzberg SL, and Leek JT (2015). Ballgown bridges the gap between transcriptome assembly and expression analysis. Nat. Biotechnol 33, 243–246. 10.1038/nbt.3172. [PubMed: 25748911]

Fullwood MJ, and Ruan Y (2009). ChIP-based methods for the identification of long-range chromatin interactions. J. Cell Biochem 107, 30–39. 10.1002/jcb.22116. [PubMed: 19247990]

Giles N, Forrest A, and Gabrielli B (2003). 14-3-3 acts as an intramolecular bridge to regulate cdc25B localization and activity. J. Biol. Chem 278, 28580–28587. 10.1074/jbc.M304027200. [PubMed: 12764136]

Graff J, Joseph NF, Horn ME, Samiei A, Meng J, Seo J, Rei D, Bero AW, Phan TX, Wagner F, et al. (2014). Epigenetic priming of memory updating during reconsolidation to attenuate remote fear memories. Cell 156, 261–276. 10.1016/j.cell.2013.12.020. [PubMed: 24439381]

Grinman E, Nakahata Y, Avchalumov Y, Espadas I, Swarnkar S, Yasuda R, and Puthanveettil SV (2021). Activity-regulated synaptic targeting of lncRNA ADEPTR mediates structural plasticity by localizing Sptn1 and AnkB in dendrites. Sci. Adv 7. 10.1126/sciadv.abf0605.

Gross C, Chang CW, Kelly SM, Bhattacharya A, McBride SM, Danielson SW, Jiang MQ, Chan CB, Ye K, Gibson JR, et al. (2015). Increased expression of the PI3K enhancer PIKE mediates deficits in synaptic plasticity and behavior in fragile X syndrome. Cell Rep. 11, 727–736. 10.1016/j.celrep.2015.03.060. [PubMed: 25921541]

Hagege H, Klous P, Braem C, Splinter E, Dekker J, Cathala G, de Laat W, and Forne T (2007). Quantitative analysis of chromosome conformation capture assays (3C-qPCR). Nat. Protoc 2, 1722–1733. 10.1038/nprot.2007.243. [PubMed: 17641637]

Halder R, Hennion M, Vidal RO, Shomroni O, Rahman RU, Rajput A, Centeno TP, van Bebber F, Capece V, Garcia Vizcaino JC, et al. (2016). DNA methylation changes in plasticity genes accompany the formation and maintenance of memory. Nat. Neurosci 19, 102–110. 10.1038/nn.4194. [PubMed: 26656643]

Hollensen AK, Thomsen HS, Lloret-Llinares M, Kamstrup AB, Jensen JM, Luckmann M, Birkmose N, Palmfeldt J, Jensen TH, Hansen TB, and Damgaard CK (2020). circZNF827 nucleates a transcription inhibitory complex to balance neuronal differentiation. Elife 9. 10.7554/eLife.58478.

Hughes BW, Siemsen BM, Berto S, Kumar J, Cornbrooks RG, Akiki RM, Carter JS, Scofield MD, Cowan CW, and Taniguchi M (2021). NPAS4 in the medial prefrontal cortex mediates chronic social defeat stress-induced anhedonia and dendritic spine loss. Preprint at bioRxiv. 10.1101/2021.03.04.433930.

Issler O, van der Zee YY, Ramakrishnan A, Wang J, Tan C, Loh YE, Purushothaman I, Walker DM, Lorsch ZS, Hamilton PJ, et al. (2020). Sex-specific role for the long non-coding RNA LINC00473 in depression. Neuron 106, 912–926.e915. 10.1016/j.neuron.2020.03.023. [PubMed: 32304628]

Jeon Y, and Lee JT (2011). YY1 tethers Xist RNA to the inactive X nucleation center. Cell 146, 119–133. 10.1016/j.cell.2011.06.026. [PubMed: 21729784]

Kim D, Paggi JM, Park C, Bennett C, and Salzberg SL (2019). Graph-based genome alignment and genotyping with HISAT2 and HISAT-genotype. Nat. Biotechnol 37, 907–915. 10.1038/s41587-019-0201-4. [PubMed: 31375807]

Kim D, Langmead B, and Salzberg SL (2015a). HISAT: a fast spliced aligner with low memory requirements. Nat. Methods 12, 357–360. 10.1038/nmeth.3317. [PubMed: 25751142]

Kim TK, Hemberg M, and Gray JM (2015b). Enhancer RNAs: a class of long noncoding RNAs synthesized at enhancers. Cold Spring Harb. Perspect. Biol 7, a018622. 10.1101/cshperspect.a018622. [PubMed: 25561718]

Kim TK, Hemberg M, Gray JM, Costa AM, Bear DM, Wu J, Harmin DA, Laptewicz M, Barbara-Haley K, Kuersten S, et al. (2010). Widespread transcription at neuronal activity-regulated enhancers. Nature 465, 182–187. 10.1038/nature09033. [PubMed: 20393465]

Kukharsky MS, Ninkina NN, An H, Telezhkin V, Wei W, Meritens CR, Cooper-Knock J, Nakagawa S, Hirose T, Buchman VL, and Shelkovnikova TA (2020). Long non-coding RNA Neat1

regulates adaptive behavioural response to stress in mice. Transl. Psychiatry 10, 171. 10.1038/s41398-020-0854-2. [PubMed: 32467583]

Labonte B, Abdallah K, Maussion G, Yerko V, Yang J, Bittar T, Quessy F, Golden SA, Navarro L, Checknita D, et al. (2021). Regulation of impulsive and aggressive behaviours by a novel lncRNA. Mol. Psychiatry 26, 3751–3764. 10.1038/s41380-019-0637-4. [PubMed: 31907380]

Lepack AE, Werner CT, Stewart AF, Fulton SL, Zhong P, Farrelly LA, Smith ACW, Ramakrishnan A, Lyu Y, Bastle RM, et al. (2020). Dopaminylation of histone H3 in ventral tegmental area regulates cocaine seeking. Science 368, 197–201. 10.1126/science.aaw8806. [PubMed: 32273471]

Li D, Zhang J, Wang M, Li X, Gong H, Tang H, Chen L, Wan L, and Liu Q (2018). Activity dependent LoNA regulates translation by coordinating rRNA transcription and methylation. Nat. Commun 9, 1726. 10.1038/s41467-018-04072-4. [PubMed: 29712923]

Li H, and Durbin R (2009). Fast and accurate short read alignment with Burrows-Wheeler transform. Bioinformatics 25, 1754–1760. 10.1093/bioinformatics/btp324. [PubMed: 19451168]

Li H, Handsaker B, Wysoker A, Fennell T, Ruan J, Homer N, Marth G, Abecasis G, Durbin R, and 1000 Genome Project Data Processing Sub-group. (2009). The sequence alignment/map format and SAMtools. Bioinformatics 25, 2078–2079. 10.1093/bioinformatics/btp352. [PubMed: 19505943]

Li X, Wei W, Zhao QY, Widagdo J, Baker-Andresen D, Flavell CR, D'Alessio A, Zhang Y, and Bredy TW (2014). Neocortical Tet3-mediated accumulation of 5-hydroxymethylcytosine promotes rapid behavioral adaptation. Proc. Natl. Acad. Sci. U S A 111, 7120–7125. 10.1073/pnas.1318906111. [PubMed: 24757058]

Li X, Zhao Q, Wei W, Lin Q, Magnan C, Emami MR, Wearick-Silva LE, Viola TW, Marshall PR, Yin J, et al. (2019). The DNA modification N6-methyl-2'-deoxyadenosine (m6dA) drives activity-induced gene expression and is required for fear extinction. Nat. Neurosci 22, 534–544. 10.1038/s41593-019-0339-x. [PubMed: 30778148]

Li Y, Syed J, and Sugiyama H (2016). RNA-DNA triplex formation by long noncoding RNAs. Cell Chem. Biol 23, 1325–1333. 10.1016/j.chembiol.2016.09.011. [PubMed: 27773629]

Liau WS, Samaddar S, Banerjee S, and Bredy TW (2021). On the functional relevance of spatiotemporally-specific patterns of experience-dependent long noncoding RNA expression in the brain. RNA Biol. 18, 1025–1036. 10.1080/15476286.2020.1868165. [PubMed: 33397182]

Lin Q, Wei W, Coelho CM, Li X, Baker-Andresen D, Dudley K, Ratnu VS, Boskovic Z, Kobor MS, Sun YE, and Bredy TW (2011). The brain-specific microRNA miR-128b regulates the formation of fear-extinction memory. Nat. Neurosci 14, 1115–1117. 10.1038/nn.2891. [PubMed: 21841775]

Liu N, Zhou KI, Parisien M, Dai Q, Diatchenko L, and Pan T (2017). N6-methyladenosine alters RNA structure to regulate binding of a low-complexity protein. Nucleic Acids Res. 45, 6051–6063. 10.1093/nar/gkx141. [PubMed: 28334903]

Ma M, Xiong W, Hu F, Deng MF, Huang X, Chen JG, Man HY, Lu Y, Liu D, and Zhu LQ (2020). A novel pathway regulates social hierarchy via lncRNA AtLAS and postsynaptic synapsin IIb. Cell Res. 30, 105–118. 10.1038/s41422-020-0273-1. [PubMed: 31959917]

Malik AN, Vierbuchen T, Hemberg M, Rubin AA, Ling E, Couch CH, Stroud H, Spiegel I, Farh KK, Harmin DA, and Greenberg ME (2014). Genome-wide identification and characterization of functional neuronal activity-dependent enhancers. Nat. Neurosci 17, 1330–1339. 10.1038/nn.3808. [PubMed: 25195102]

Marshall PR, and Bredy TW (2019). Neuroepigenetic mechanisms underlying fear extinction: emerging concepts. Psychopharmacology (Berl) 236, 133–142. 10.1007/s00213-018-5084-4. [PubMed: 30506235]

Marshall PR, Zhao Q, Li X, Wei W, Periyakaruppiah A, Zajaczkowski EL, Leighton LJ, Madugalle SU, Basic D, Wang Z, et al. (2020). Dynamic regulation of Z-DNA in the mouse prefrontal cortex by the RNA-editing enzyme Adar1 is required for fear extinction. Nat. Neurosci 23, 718–729. 10.1038/s41593-020-0627-5. [PubMed: 32367065]

Martin H, Rostas J, Patel Y, and Aitken A (1994). Subcellular localisation of 14-3-3 isoforms in rat brain using specific antibodies. J. Neurochem 63, 2259–2265. 10.1046/j.1471-4159.1994.63062259.x. [PubMed: 7964746]

Martin SJ, Grimwood PD, and Morris RG (2000). Synaptic plasticity and memory: an evaluation of the hypothesis. Annu. Rev. Neurosci 23, 649–711. 10.1146/annurev.neuro.23.1.649. [PubMed: 10845078]

Marzinke MA, Mavencamp T, Duratinsky J, and Clagett-Dame M (2013). 14-3-3epsilon and NAV2 interact to regulate neurite outgrowth and axon elongation. Arch. Biochem. Biophys 540, 94–100. 10.1016/j.abb.2013.10.012. [PubMed: 24161943]

McKinsey TA, Zhang CL, Lu J, and Olson EN (2000). Signal-dependent nuclear export of a histone deacetylase regulates muscle differentiation. Nature 408, 106–111. 10.1038/35040593. [PubMed: 11081517]

McNulty SE, Barrett RM, Vogel-Ciernia A, Malvaez M, Hernandez N, Davatolhagh MF, Matheos DP, Schiffman A, and Wood MA (2012). Differential roles for Nr4a1 and Nr4a2 in object location vs. object recognition long-term memory. Learn. Mem 19, 588–592. 10.1101/lm.026385.112. [PubMed: 23161447]

McQuown SC, Barrett RM, Matheos DP, Post RJ, Rogge GA, Alenghat T, Mullican SE, Jones S, Rusche JR, Lazar MA, and Wood MA (2011). HDAC3 is a critical negative regulator of long-term memory formation. J. Neurosci 31, 764–774. 10.1523/JNEUROSCI.5052-10.2011. [PubMed: 21228185]

Mercer TR, Clark MB, Crawford J, Brunck ME, Gerhardt DJ, Taft RJ, Nielsen LK, Dinger ME, and Mattick JS (2014). Targeted sequencing for gene discovery and quantification using RNA CaptureSeq. Nat. Protoc 9, 989–1009. 10.1038/nprot.2014.058. [PubMed: 24705597]

Mercer TR, Dinger ME, Sunkin SM, Mehler MF, and Mattick JS (2008). Specific expression of long noncoding RNAs in the mouse brain. Proc. Natl. Acad. Sci. U S A 105, 716–721. 10.1073/pnas.0706729105. [PubMed: 18184812]

Mercer TR, Gerhardt DJ, Dinger ME, Crawford J, Trapnell C, Jeddeloh JA, Mattick JS, and Rinn JL (2011). Targeted RNA sequencing reveals the deep complexity of the human transcriptome. Nat. Biotechnol 30, 99–104. 10.1038/nbt.2024. [PubMed: 22081020]

Mercer TR, and Mattick JS (2013). Structure and function of long noncoding RNAs in epigenetic regulation. Nat. Struct. Mol. Biol 20, 300–307. 10.1038/nsmb.2480. [PubMed: 23463315]

Perry RB, Hezroni H, Goldrich MJ, and Ulitsky I (2018). Regulation of neuroregeneration by long noncoding RNAs. Mol. Cell 72, 553–567.e555. 10.1016/j.molcel.2018.09.021. [PubMed: 30401432]

Pertea M, Pertea GM, Antonescu CM, Chang TC, Mendell JT, and Salzberg SL (2015). StringTie enables improved reconstruction of a transcriptome from RNA-seq reads. Nat. Biotechnol 33, 290–295. 10.1038/nbt.3122. [PubMed: 25690850]

Qiao H, Foote M, Graham K, Wu Y, and Zhou Y (2014). 14-3-3 proteins are required for hippocampal long-term potentiation and associative learning and memory. J. Neurosci 34, 4801–4808. 10.1523/JNEURO-SCI.4393-13.2014. [PubMed: 24695700]

Quinlan AR, and Hall IM (2010). BEDTools: a flexible suite of utilities for comparing genomic features. Bioinformatics 26, 841–842. 10.1093/bioinformatics/btq033. [PubMed: 20110278]

Raveendra BL, Swarnkar S, Avchalumov Y, Liu XA, Grinman E, Badal K, Reich A, Pascal BD, and Puthanveettil SV (2018). Long noncoding RNA GM12371 acts as a transcriptional regulator of synapse function. Proc. Natl. Acad. Sci. U S A 115, E10197–E10205. 10.1073/pnas.1722587115. [PubMed: 30297415]

Salatino-Oliveira A, Wagner F, Akutagava-Martins GC, Bruxel EM, Genro JP, Zeni C, Kieling C, Polanczyk GV, Rohde LA, and Hutz MH (2016). MAP1B and NOS1 genes are associated with working memory in youths with attention-deficit/hyperactivity disorder. Eur. Arch. Psychiatry Clin. Neurosci 266, 359–366. 10.1007/s00406-015-0626-9. [PubMed: 26233433]

Sando R 3rd, Gounko N, Pieraut S, Liao L, Yates J 3rd, and Maximov A (2012). HDAC4 governs a transcriptional program essential for synaptic plasticity and memory. Cell 151, 821–834. 10.1016/j.cell.2012.09.037. [PubMed: 23141539]

Schaukowitch K, Joo JY, Liu X, Watts JK, Martinez C, and Kim TK (2014). Enhancer RNA facilitates NELF release from immediate early genes. Mol Cell 56, 29–42. 10.1016/j.molcel.2014.08.023. [PubMed: 25263592]

Seiler J, Breinig M, Caudron-Herger M, Polycarpou-Schwarz M, Boutros M, and Diederichs S (2017). The lncRNA VELUCT strongly regulates viability of lung cancer cells despite its extremely low abundance. Nucleic Acids Res. 45, 5458–5469. 10.1093/nar/gkx076. [PubMed: 28160600]

Shanmugam R, Zhang F, Srinivasan H, Charles Richard JL, Liu KI, Zhang X, Woo CWA, Chua ZHM, Buschdorf JP, Meaney MJ, and Tan MH (2018). SRSF9 selectively represses ADAR2-mediated editing of brain-specific sites in primates. Nucleic Acids Res. 46, 7379–7395. 10.1093/nar/gky615. [PubMed: 29992293]

Spadaro PA, and Bredy TW (2012). Emerging role of non-coding RNA in neural plasticity, cognitive function, and neuropsychiatric disorders. Front. Genet 3, 132. 10.3389/fgene.2012.00132. [PubMed: 22811697]

Spadaro PA, Flavell CR, Widagdo J, Ratnu VS, Troup M, Ragan C, Mattick JS, and Bredy TW (2015). Long noncoding RNA-directed epigenetic regulation of gene expression is associated with anxiety-like behavior in mice. Biol. Psychiatry 78, 848–859. 10.1016/j.biopsych.2015.02.004. [PubMed: 25792222]

Tang WH, Shilov IV, and Seymour SL (2008). Nonlinear fitting method for determining local false discovery rates from decoy database searches. J. Proteome Res 7, 3661–3667. 10.1021/pr070492f. [PubMed: 18700793]

Vecsey CG, Hawk JD, Lattal KM, Stein JM, Fabian SA, Attner MA, Cabrera SM, McDonough CB, Brindle PK, Abel T, and Wood MA (2007). Histone deacetylase inhibitors enhance memory and synaptic plasticity via CREB:CBP-dependent transcriptional activation. J. Neurosci 27, 6128–6140. 10.1523/JNEUROSCI.0296-07.2007. [PubMed: 17553985]

Wakeling E, McEntagart M, Bruccoleri M, Shaw-Smith C, Stals KL, Wakeling M, Barnicoat A, Beesley C, Study DDD, Hanson-Kahn AK, et al. (2021). Missense substitutions at a conserved 14-3-3 binding site in HDAC4 cause a novel intellectual disability syndrome. HGG Adv. 2, 100015. 10.1016/j.xhgg.2020.100015. [PubMed: 33537682]

Wang F, Wang Q, Liu B, Mei L, Ma S, Wang S, Wang R, Zhang Y, Niu C, Xiong Z, et al. (2021). The long noncoding RNA Synage regulates synapse stability and neuronal function in the cerebellum. Cell Death Differ. 28, 2634–2650. 10.1038/s41418-021-00774-3. [PubMed: 33762741]

Wang X, Cairns MJ, and Yan J (2019). Super-enhancers in transcriptional regulation and genome organization. Nucleic Acids Res. 47, 11481–11496. 10.1093/nar/gkz1038. [PubMed: 31724731]

Wei W, Coelho CM, Li X, Marek R, Yan S, Anderson S, Meyers D, Mukherjee C, Sbardella G, Castellano S, et al. (2012). p300/CBP-associated factor selectively regulates the extinction of conditioned fear. J. Neurosci 32, 11930–11941. 10.1523/JNEUROSCI.0178-12.2012. [PubMed: 22933779]

Wu Q, and Yi X (2018). Down-regulation of long noncoding RNA MALAT1 protects hippocampal neurons against excessive autophagy and apoptosis via the PI3K/akt signaling pathway in rats with epilepsy. J. Mol. Neurosci 65, 234–245. 10.1007/s12031-018-1093-3. [PubMed: 29858824]

Xiong Z, Lo HP, McMahon KA, Martel N, Jones A, Hill MM, Parton RG, and Hall TE (2021). In vivo proteomic mapping through GFP-directed proximity-dependent biotin labelling in zebrafish. Elife 10. 10.7554/eLife.64631.

Xu H, Brown AN, Waddell NJ, Liu X, Kaplan GJ, Chitaman JM, Stockman V, Hedinger RL, Adams R, Abreu K, et al. (2020). Role of long noncoding RNA Gas5 in cocaine action. Biol. Psychiatry 88, 758–766. 10.1016/j.biopsych.2020.05.004. [PubMed: 32711952]

Yamazaki T, Souquere S, Chujo T, Kobelke S, Chong YS, Fox AH, Bond CS, Nakagawa S, Pierron G, and Hirose T (2018). Functional domains of NEAT1 architectural lncRNA induce paraspeckle assembly through phase separation. Mol. Cell 70, 1038–1053.e1037. 10.1016/j.molcel.2018.05.019. [PubMed: 29932899]

Zhang J, and Zhou Y (2018). 14-3-3 proteins in glutamatergic synapses. Neural Plast. 2018, 8407609. 10.1155/2018/8407609. [PubMed: 29849571]

Zhang Y, Liu T, Meyer CA, Eeckhoute J, Johnson DS, Bernstein BE, Nusbaum C, Myers RM, Brown M, Li W, and Liu XS (2008). Model-based analysis of ChIP-seq (MACS). Genome Biol. 9, R137. 10.1186/gb-2008-9-9-r137. [PubMed: 18798982]

Zhu Y, Huang M, Bushong E, Phan S, Uytiepo M, Beutter E, Boemer D, Tsui K, Ellisman M, and Maximov A (2019). Class IIa HDACs regulate learning and memory through dynamic experience-

dependent repression of transcription. Nat. Commun 10, 3469. 10.1038/s41467-019-11409-0. [PubMed: 31375688]

Highlights

- Targeted RNA sequencing reveals learning-induced lncRNAs in the adult brain
- ADRAM is critical for the formation of fear extinction memory
- ADRAM coordinates the epigenomic regulation of Nr4a2

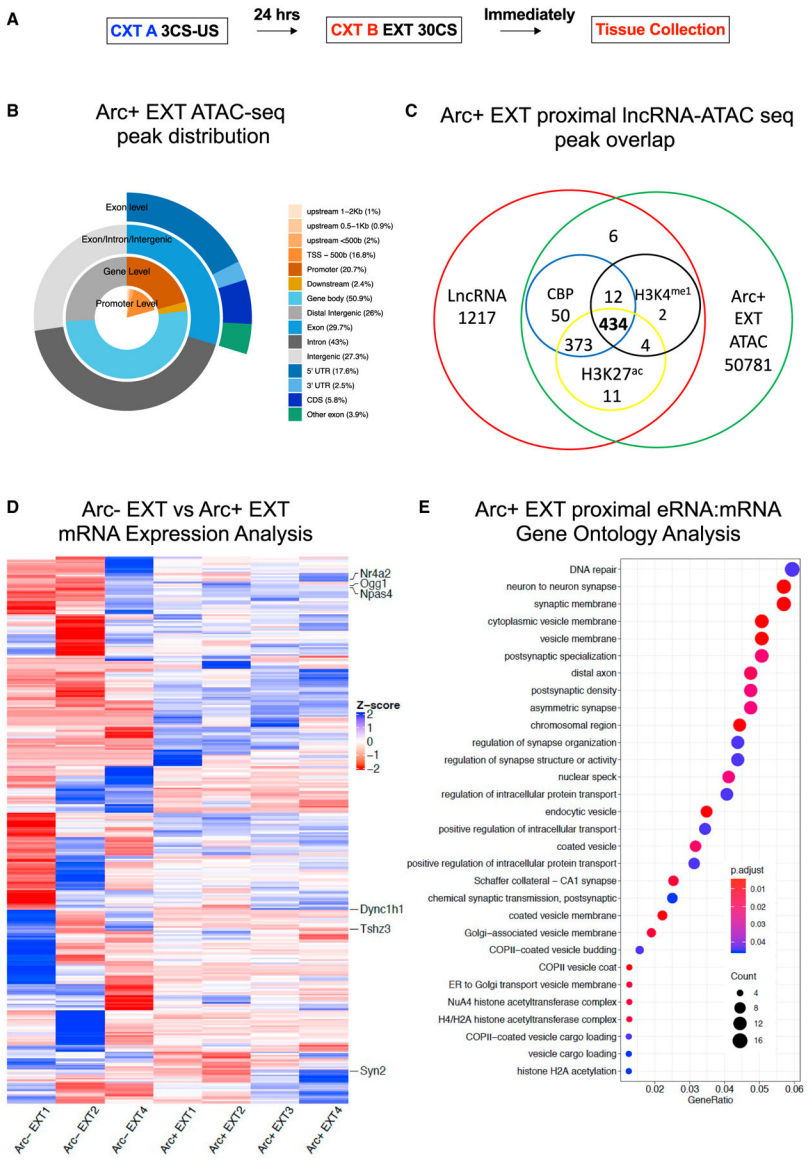

Figure 1. LncRNAs derived from enhancer elements are induced by fear extinction learning and correlate with proximal protein-coding gene expression in the adult prefrontal cortex

(A) Schematic of the behavioral protocol used to collect ILPFC tissue after fear extinction training.

(B) Genomic distribution of ATAC peaks in Arc+ neurons that have been activated by fear extinction learning.

(C) The Venn diagram highlights 434 proximal lncRNAs overlapping with lncRNA capture-seq, Arc+ EXT ATAC-seq, as well as H3K27^{ac}-, CBP-, and H3K4^{me1}-enriched genomic regions.

(D) Heatmap of eRNA-associated mRNA expression in quiescent (ARC−EXT) versus activated (ARC+ EXT) neurons (n = 3 biological replicates for ARC− EXT; n = 4 biological replicates ARC+ EXT; red, decreased expression; blue, increase expression).

(E) Gene ontology (GO) analysis for proximal protein-coding genes located <10 kb downstream of the 434 eRNA loci. The top 30 significantly enriched GO terms are shown in the dot plot.

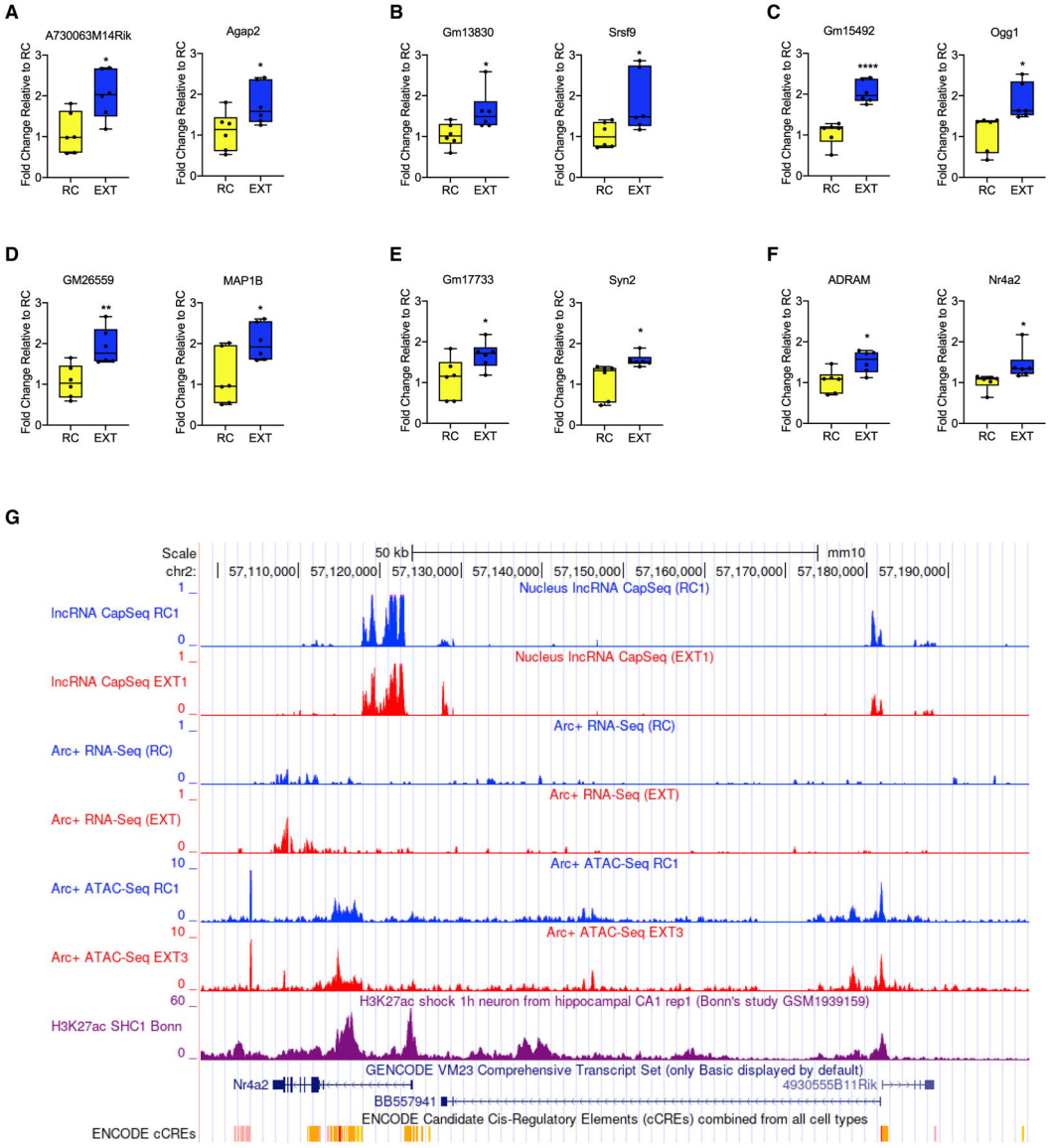

Figure 2. Extinction training leads to an increase in the expression of proximal eRNAs and their downstream mRNAs

(A–F) (A) A730063M14Rik:Agap2, (B) Gm17733:Syn2, (C) Gm15492:Ogg1, (D) Gm26559:Map1b, (E) Gm13830:Srsf9, and (F) BB557941:Nr4a2 (n = 6 biological replicates per group, two-tailed unpaired Student's t test). Error bars represent SEM; *p < 0.05, **p < 0.01, ****p < 0.0001.

(G) Representative UCSC genome browser track showing ADRAM, Nr4a2, and H3K27^{ac} peaks in RC and EXT mice.

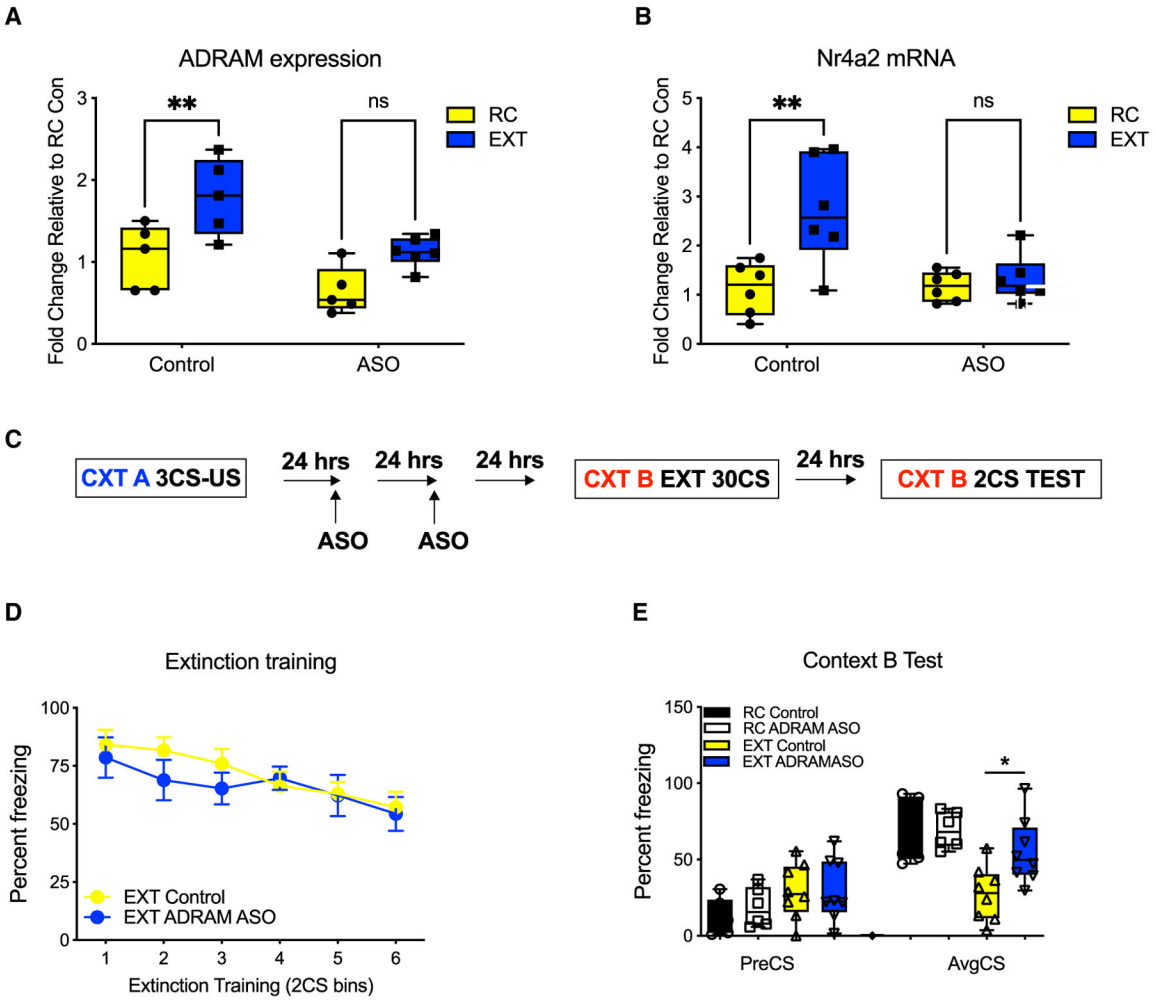

Figure 3. Learning-induced ADRAM expression is necessary for the induction of the immediate-early gene Nr4a2 and is required for fear extinction memory

(A and B) (A) ADRAM ASO blocks the extinction-learning-induced induction of ADRAM expression (n = 5–6 biological replicates per group, two-way ANOVA, $F(1,17) = 13.18$, Šídák's post hoc analysis, Control RC versus Control EXT, $p = 0.0070$) and (B) Nr4a2 mRNA expression (n = 6 biological replicates per group, two-way ANOVA, $F(1,20) = 5.989$, Šídák's post hoc analysis, Control RC versus Control EXT, $p = 0.0012$).

(C) Schematic of the behavioral protocol used to test the effect of the ADRAM ASO in the ILPFC on fear extinction memory.

(D) There were no significant differences between the ADRAM ASO and control groups during fear acquisition, and no effect of ADRAM ASO on performance during within-session extinction training.

(E) However, knockdown of ADRAM led to a significant impairment in memory for fear extinction (n = 8 animals per group, one-way ANOVA, $F(3,14) = 8.098$, Šídák's post hoc analysis, Con EXT versus ASO EXT, $p = 0.0313$). CS, conditioned stimulus; preCS, a 2 min acclimation pretest period to minimize context generalization; AvgCS, average of 2 tone CS exposures, at test. Error bars represent SEM; *$p < 0.05$, **$p < 0.01$.

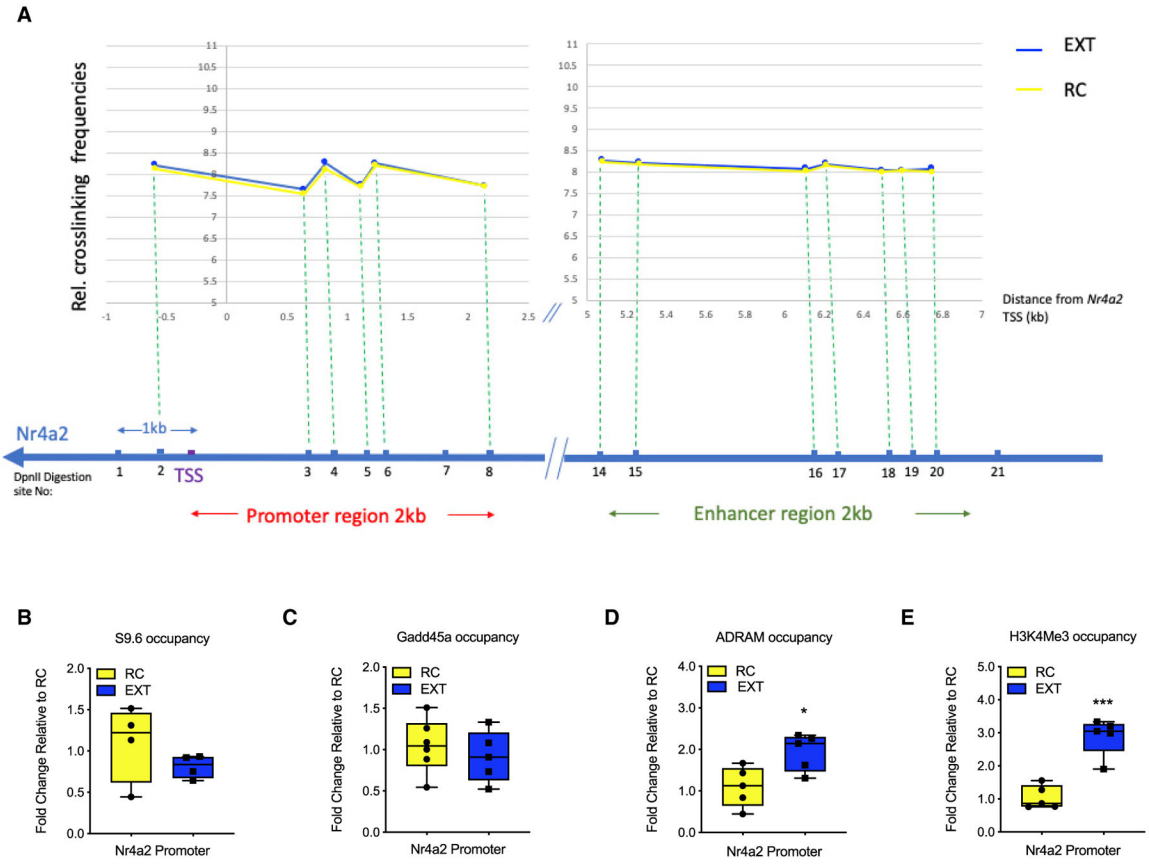

Figure 4. ADRAM regulates the induction of the immediate-early gene Nr4a2 via a direct interaction with the Nr4a2 promoter

(A) 3C-qPCR analysis of long-distance interactions at the mouse NR4A2 locus. The relative level of each ligation product (fragments −1 to 8 and 14 to 20) has been plotted according to its distance (in kb) from the Nr4a2 promoter. The data were normalized to GAPDH. Below the graphs, the TaqII restriction fragments are indicated. TaqII fragments are numbered from fragment −1 to 21.

(B) DRIP experiment using S9.6 antibody showing no difference in S9.6 occupancy in the Nr4a2 promoter region in RC compared with EXT mice.

(C) There was no significant difference in Gadd45a occupancy at the Nr4a2 promoter.

(D and E) (D) ChIRP experiment demonstrating ADRAM binding to the Nr4a2 promoter in EXT mice (n = 5 biological replicates per group, two-tailed unpaired Student's t test), which is accompanied by an increase in H3K4me3 occupancy (E) (n = 5 biological replicates per group, two-tailed unpaired Student's t test). Error bars represent SEM; *p < 0.05, ***p < 0.001.

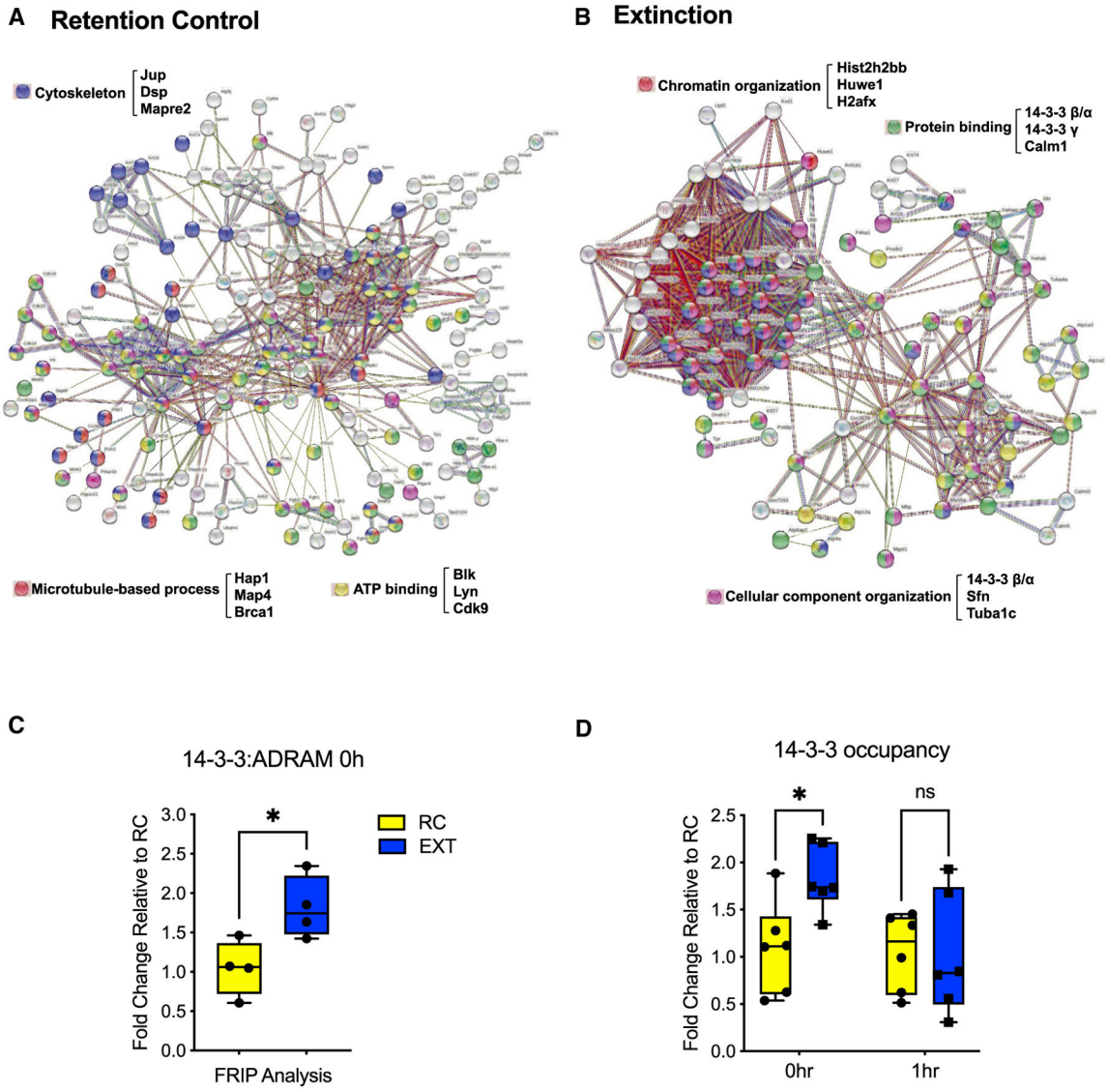

Figure 5. ADRAM serves as both a guide and a scaffold to coordinate fear extinction learning-induced occupancy of 14-3-3 at the Nr4a2 promoter

(A and B) Representative functional interaction networks analysis of ADRAM interacting proteins in (A) RC and (B) EXT mice.

(C) 14-3-3β/α formaldehyde-RNA immunoprecipitation (fRIP) shows increased binding of 14-3-3β/α to ADRAM in EXT mice (n = 5 biological replicates per group, two-tailed unpaired Student's t test).

(D) 14-3-3β/α chIP-qPCR reveals a transient change 14-3-3 occupancy at the Nr4a2 promoter post-extinction training (n = 6 biological replicates per group, two-way ANOVA, $F(1,20) = 4.589$, Šídák's post hoc analysis, 0 h RC versus 0 h EXT, $p = 0.0309$). Error bars represent SEM; *$p < 0.05$.

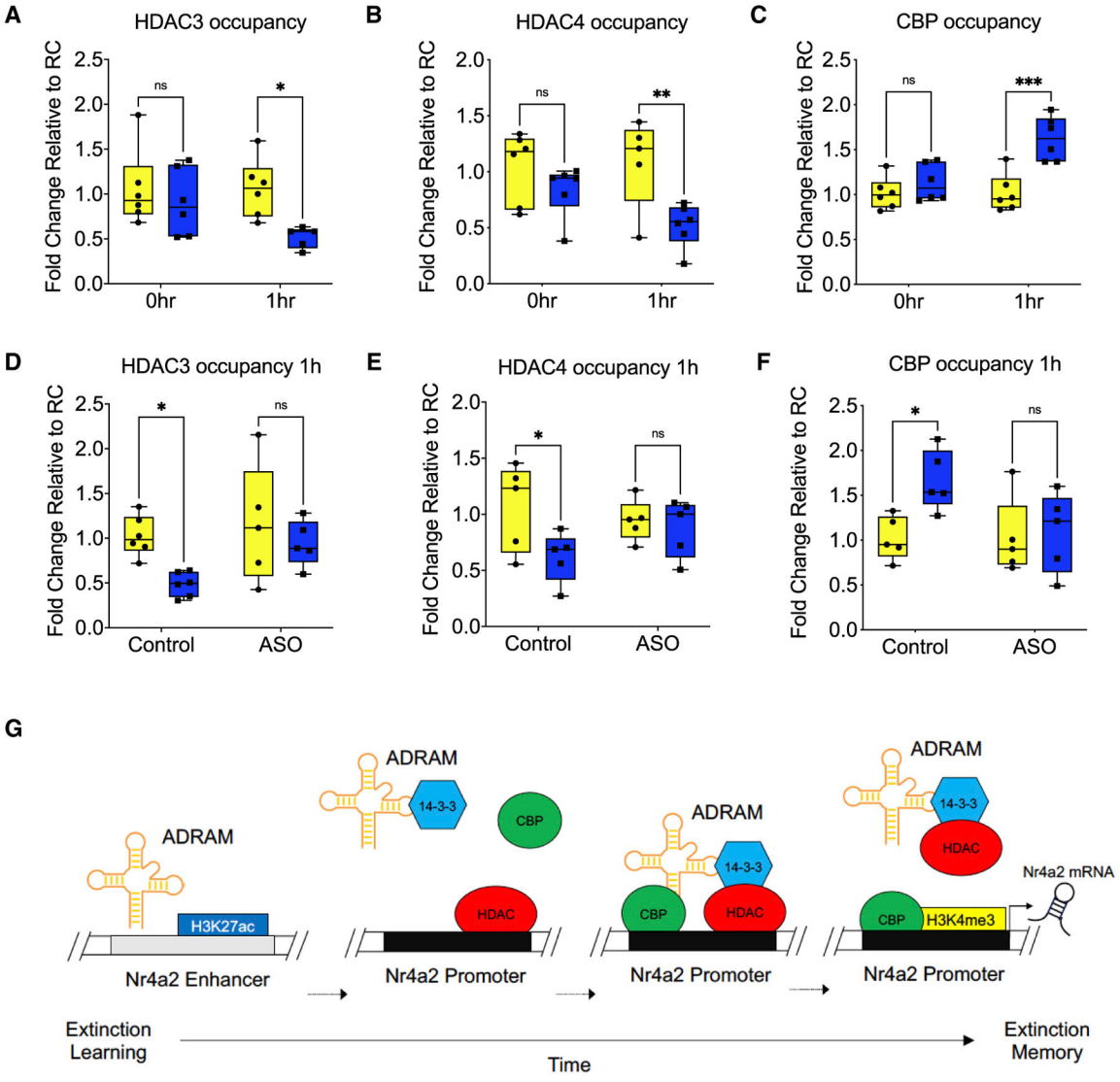

Figure 6. Learning-induced recruitment of 14-3-3 leads to a time-dependent change in the activity of chromatin modifiers at Nr4a2 promoter

(A and B) ChIP-qPCR shows a reduction in both (A) HDAC3 (n = 5–6 biological replicates per group, two-way ANOVA, $F(1,19) = 5.900$, Šídák's post hoc analysis, 1 h RC versus 1 h EXT, $p = 0.0328$) and (B) HDAC4 at the Nr4a2 promoter 1 h post EXT (n = 5–6 biological replicates per group, two-way ANOVA, $F(1,19) = 10.06$, Šídák's post hoc analysis, 1 h RC versus 1 h EXT, $p = 0.0001$).

(C–F) (C) In contrast, there was a significant increase in CBP occupancy at the Nr4a2 promoter 1 h after extinction training (n = 6 biological replicates per group, two-way ANOVA, $F(1,20) = 8.273$, Šídák's post hoc analysis, 1 h RC versus 1 h EXT, $p = 0.0328$). All of the above effects were prevented in mice that had been treated with antisense oligonucleotides directed to ADRAM, (D) HDAC3 (n = 5–6 biological replicates per group, two-way ANOVA, $F(1,18) = 5.815$, Šídák's post hoc analysis, Con RC versus Con EXT, $p = 0.0375$), (E) HDAC4 (n = 5 biologically independent animals per group, two-way ANOVA, $F(1,16) = 4.339$, Šídák's post hoc analysis, Control RC versus Control EXT, $p = 0.0404$),

and (F) CBP (n = 5 biological replicates per group, two-way ANOVA, $F(1,16) = 4.520$, Šídák's post hoc analysis, Control RC versus Control EXT, $p = 0.0291$).
(G) Proposed model of ADRAM-mediated regulation of epigenomic machinery underlying fear extinction learning-induced Nr4a2 expression. Error bars represent SEM; *$p < 0.05$, **$p < 0.01$, ***$p < 0.001$.

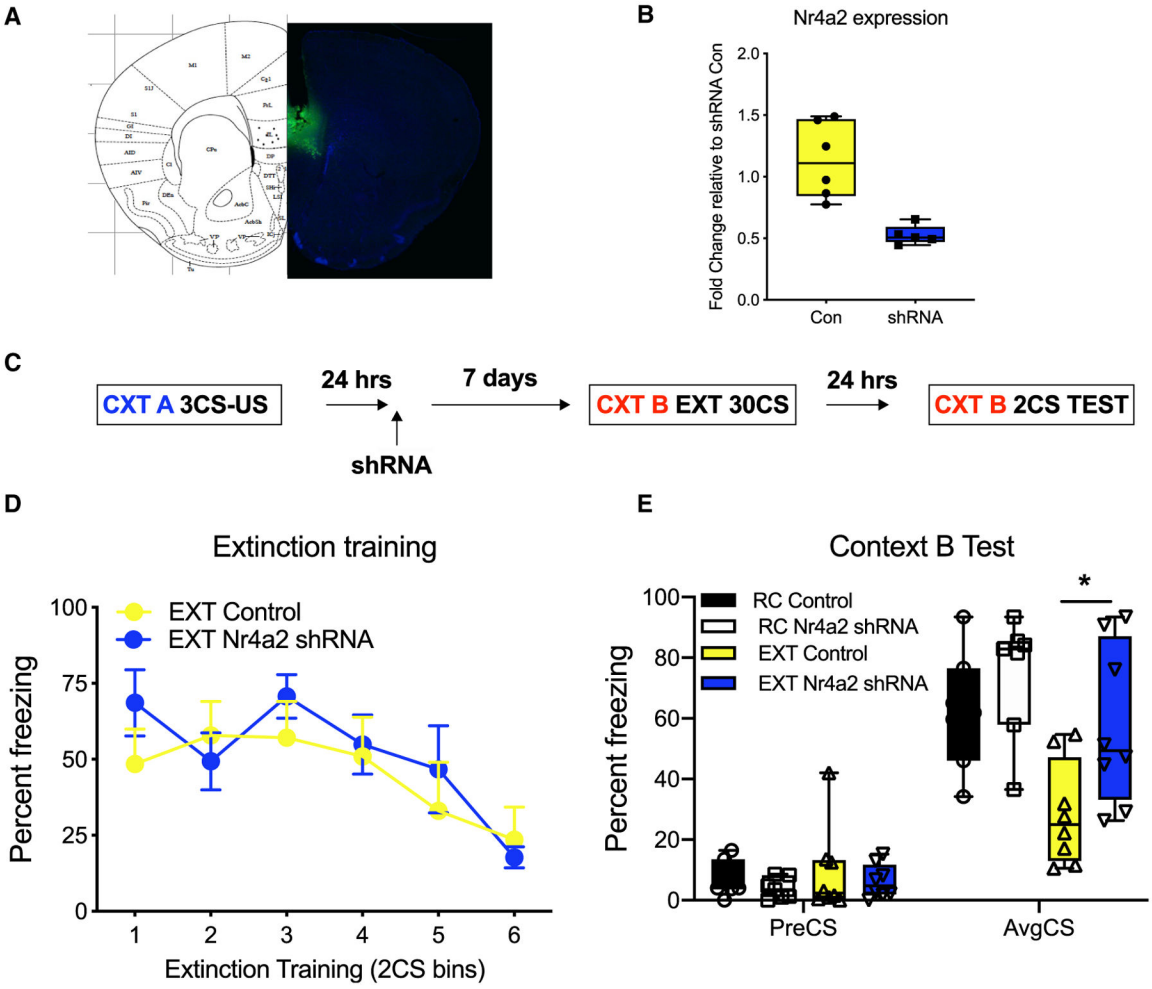

Figure 7. Nr4a2 expression is necessary for the formation of fear extinction memory

(A) Representative image of viral infection of Nr4a2 shRNA lentivirus into the ILPFC.

(B) qRT-PCR shows significant Nr4a2 mRNA knockdown following Nr4a2 shRNA injection in the ILPFC (n = 5–6 biological replicates per group, two-tailed unpaired Student's t test).

(C) Schematic of the behavioral protocol used to test the effect of Nr4a2 shRNA on fear extinction memory.

(D) There was no effect of Nr4a2 knockdown on performance during within-session extinction training.

(E) Nr4a2 knockdown led to a significant impairment in memory for fear extinction (n = 8 animals per group, one-way ANOVA, $F(3,26) = 6.574$, Šídák's post hoc analysis, Control EXT versus shRNA EXT, $p = 0.0496$). CS, conditioned stimulus; preCS, a 2 min acclimation pretest period to minimize context generalization; AvgCS, average of 2 tone CS exposures, at test. Error bars represent SEM; *$p < 0.05$.

KEY RESOURCES TABLE

REAGENT or RESOURCE	SOURCE	IDENTIFIER
Antibodies		
Rabbit anti-H3K4me3	Active motif	39915
Rabbit anti-H3K27ac	Active motif	39685
Rabbit anti-CBP	Abcam	ab10489
Rabbit anti-S9.6	Merck	MABE1095
Rabbit anti-Gadd45a	Cell Signaling	4632
Rabbit anti-14-3-3 β/α	Cell Signaling	9636
Rabbit anti-NeuN-488	Abcam	Ab190195
Rabbit anti-Arc-647	Bioss	BS-0385R-A647
Rabbit anti-MAP2	Abcam	ab32454
Rabbit anti-HDAC3	Active motif	40968
Rabbit anti-HDAC4	Active motif	40969
Mouse anti-β-Tubulin	Cell Signaling	86298
Bacterial and virus strains		
One Shot™ Stbl3™ Chemically Competent E. coli	Thermo Fisher	C737303
Chemicals, peptides, and recombinant proteins		
Ketamine	Parchem	100477-72-3
Xylazine hydrochloride	MERCK	23076-35-9
Chloroform	MERCK	319988
Tween 20	MERCK	P1379
Paraformaldehyde	MERCK	158127
Pierce™ 16% Formaldehyde (w/v), Methanol-free	Thermo Fisher	28908
Glycine	MERCK	50046
Proteinase K	NEB	P8107S
Phenol:Chloroform:Isoamyl Alcohol 25:24:1	MERCK	P3803
Sodium butyrate	MERCK	B5887
Ethyl alcohol, Pure	MERCK	459836
Triton™ X-100 solution	MERCK	93443
cOmplete protease inhibitor cocktail tablets	Roche	5056489001
10% SDS	MERCK	71736
$NaHCO_3$	MERCK	S6014
Papain	Worthington	LS003126
B-27	Thermo Fisher	17504044
GlutaMax	Thermo Fisher	35050061
Neurobasal™ Medium	Thermo Fisher	21103049
DMEM, high glucose	Thermo Fisher	11965092
Opti-MEM™ I Reduced Serum Medium	Thermo Fisher	11058021
Pen/Strep	Thermo Fisher	15140122
NP40 Cell Lysis Buffer	Thermo Fisher	FNN0021

REAGENT or RESOURCE	SOURCE	IDENTIFIER
Novex 4 to 12%, Tris-Glycine Gel	Thermo Fisher	XV04120PK20
DNase I	Thermo Fisher	18047019
Normal Goat Serum	Thermo Fisher	31872
Poly-L- Ornithine	MERCK	P2533
TRIS hydrochloride	MERCK	PHG0002
NaCl	MERCK	S9888
$MgCl_2$	MERCK	M8266
Igepal CA-630	MERCK	I8896
DpnII	NEB	R0543
Biotin	MERCK	B4501
HEPES	MERCK	54457
Sarkosyl	MERCK	61739
Na-Deoxycholate	MERCK	30970
TCA	MERCK	T6399
Lipofectamine	Thermo Fisher	18324012
PageRuler™ Prestained Protein Ladder	Thermo Fisher	26616
Isopropanol	MERCK	I9516
Critical commercial assays		
DNeasy Blood & Tissue Kit	Qiagen	69504
TRIzol™ Reagent	Thermo Fisher	15596018
Qubit™ dsDNA HS Assay Kits	Thermo Fisher	Q32851
Qubit™ RNA high sensitivity (HS) Assay Kits	Thermo Fisher	Q32852
Rotor-Gene SYBR Green PCR Kit	Qiagen	204076
Dynabeads Protein G	Thermo Fisher	10004D
Dynabeads MyOne streptavidin C1	Thermo Fisher	65001
NEBNext rRNA Depletion Kit	NEB	E6310
NEBNext Ultra™ II RNA Library Prep Kit for Illumina	NEB	E7775
SeqCap EZ Hybridization and Wash Kit	Roche	05634261001
ATAC-Seq Kit	Active Motif	53150
PrimeScript Reverse Transcription Kit	Takara	RR014B
Deposited data		
Raw and analyzed data	This paper	GEO: GSE181706
Mouse reference genome (mm10)	Genome Reference Consortium	https://sapac.support.illumina.com/sequencing/sequencing_software/igenome.html
Experimental models: Cell lines		
HEK293T	ATCC	CRL-3216
Neuro-2a	ATCC	CCL-131
Mouse primary cortical neurons	N/A	N/A
Experimental models: Organisms/strains		
Mouse: C57BL/6	Animal Resource Centre, Western Australia	N/A
Recombinant DNA		

REAGENT or RESOURCE	SOURCE	IDENTIFIER
Mouse BAC Clone	Thermo Fisher	RP23–271B15
Software and algorithms		
HISAT2	Kim et al. (2019)	http://daehwankimlab.github.io/hisat2/
Cutadapt	https://doi.org/10.14806/ej.17.1.200	https://github.com/marcelm/cutadapt
Samtools	Li et al. (2009)	http://samtools.sourceforge.net/
StringTie	Pertea et al. (2015)	https://ccb.jhu.edu/software/stringtie/
Ballgown	Frazee et al. (2015)	https://www.bioconductor.org/packages/devel/bioc/vignettes/ballgown/inst/doc/ballgown.html
BWA	Li et al. (2009)	http://bio-bwa.sourceforge.net/bwa.shtml
BEDTools	Quinlan and Hall. (2010)	https://bedtools.readthedocs.io/en/latest/
MACS2	Zhang et al. (2008)	https://pypi.org/project/MACS2/
Other		
Double cannula	PlasticsOne	N/A